UNIVERSITY OF CALIFORNIA, SAN DIEGO

Odor Representations in Olfactory Cortex

A dissertation submitted in partial satisfaction of the

requirements for the degree Doctor of Philosophy

in

Neurosciences

by

Cindy Poo

Committee in charge:

Professor Jeffry S. Isaacson, Chair
Professor Edward M. Callaway
Professor Massimo Scanziani
Professor Jing Wang
Professor Charles S. Zuker

2011

The Dissertation of Cindy Poo is approved, and it is acceptable in quality and form for publication on microfilm and electronically:

Chair

University of California, San Diego

2011

Table of Contents

List of Figures

Introduction

Chapter 1

Chapter 2

Chapter 3

Chapter 4

Chapter 5

Acknowledgments

My deepest gratitude goes to:

Jeff Isaacson for being a mentor and a friend; for providing me with guidance, enthusiasm and support over the years. I feel extremely lucky to have had my scientific training in the Isaacson lab.

Massimo Scanziani for his kindness as a second advisor, and for promoting a collaborative and open environment between the Isaacson and Scanziani labs.

Caleb Stokes for showing up everyday, and for being a reliable source of excellent food and great fun.

All the members of the Isaacson and Scanziani labs past and present for making it a joy for me to be in lab.

Bassam Atallah for a never-ending supply of encouragement, patience, and love; for being my toughest critic and strongest supporter.

Chapter 1 is a reprint of the material as it appears in Poo C. and Isaacson, J.S. An Early Critical Period for Long-Term Plasticity and Structural Modification of Sensory Synapses in Olfactory Cortex J Neurosci. 2007 July 11; 27(28):7553-7558. The dissertation author was the primary author of this material.

Chapters 2 and 3 consists of work published in Poo C. and Isaacson, J.S. Odor representations in olfactory cortex: "sparse" coding, global inhibition and oscillations. Neuron. 2009 June 25; 62(6): 850–861. The dissertation author was the primary author of this material.

Vita

1999	B.S., Neuroscience w/ Honors, Brown University, Providence, RI
2003-2004	Research Assistant, Picower Center for Learning and Memory, MIT, Cambridge, MA
2011	Ph.D., Neurosciences, Univ. of California, San Diego, La Jolla, CA

Publications

Poo, C & Isaacson, JS (2009). Odor representations in olfactory cortex: "sparse" coding, global inhibition and oscillations. Neuron 62(6):850-61.

Poo, C & Isaacson, JS (2007). An early critical period for long-term plasticity and structural modification of olfactory synapses. Journal of Neuroscience 27(28):7553-8

Awards

2010	Leon Thal Award for Excellence in Graduate Research
2007-2010	Ruth L. Kirschstein National Research Service Award (NRSA), NIDCD
2004-2006	Merck-UCSD Neuroscience Fellowship
2003	Undergraduate Teaching and Research Award (UTRA), Brown University
1999-2003	University scholarship, Brown University

ABSTRACT OF THE DISSERTATION

Odor Representations in Olfactory Cortex

by

Cindy Poo

Doctor of Philosophy in Neurosciences

University of California, San Diego, 2011

Professor Jeffry S. Isaacson, Chair

Events in our external world are transformed into internal percepts and experiences. How can we begin to understand this transformation? It starts with the stimulation of peripheral sensory organs and ultimately requires the holistic synthesis of ensemble neural activity in the cortex. The cortex is composed of circuits connecting diverse types of neurons across various functional brain regions. In order to fully understand the cortical representation of an external stimulus, we must dissect out basic components of the circuit and characterize their stimulus response properties.

We study neural circuits in primary olfactory (piriform) cortex of rodents using electrophysiological recordings in brain slices and *in vivo*. We examine the underlying synaptic mechanisms of odor representations, and how it can be modulated. First, we demonstrate an early developmental critical period for plasticity and structural changes in principal neurons of the olfactory cortex in response to sensory afferent activity.

Next, we use in vivo recordings to demonstrate that synaptic inhibition is widely recruited by odor stimuli, whereas synaptic excitation is more selective in principal neurons. We show that the recruitment of both local interneurons as well as intracortical excitatory connections serve to shape odor-evoked synaptic activity.

Synchronous beta (15-30 Hz) oscillations between the olfactory cortex and bulb are thought to be important for odor discrimination. We find that odor-evoked synaptic currents in principle cells of olfactory cortex are couple to beta frequency oscillations in the local field potential. A time window between oscillatory synaptic excitation and inhibition restricts the spike timing of odor-evoked spikes. Beta frequency oscillations have been shown to require a centrifugal feedback loop from olfactory cortex back to the bulb. We use an optogenetic approach to reveal that cortical feedback projections provide inhibition onto mitral cells in the olfactory bulb via activation of granule cells.

This work establishes a framework to understand basic components of odor representations in olfactory cortex, and a role for cortico-bulbar feedback loop. In combination with work done in the visual, auditory, somatosensory and gustatory cortices, this study contributes to a more complete understanding of sensory information processing by cortical circuits.

Introduction

How does an animal in the wild locate food sources, avoid predators, while remembering these past experiences for future reference? The success of an animal at performing these tasks is of utmost importance for its survival. Rodents rely heavily on the olfactory system to solve many of these problems, from detection and discrimination of a food or predictor odor, to learned association of a given odor with a particular environment. In the olfactory system, the percept of an 'olfactory object' is dependent on molecular features of the odorant. In the following paragraphs, I will focus on our understanding of mammalian olfactory systems.

Olfactory bulb

Odorant molecules activate olfactory receptor neurons in the nasal olfactory epithelium and information regarding odor identity is relayed through the olfactory bulb to the olfactory cortex. Olfactory nerve fibers (carrying information from olfactory receptor neurons) form synapses onto the distal dendritic tufts of mitral and tufted cells, which are the major principal cells of the olfactory bulb. Mitral and tufted cell (M/T cell) axons coalesce below the mitral cell layer to form the lateral olfactory tract (LOT), which sends olfactory information to the olfactory cortex (Fig. I.1). In rodents, the distal dendrites of approximately 25-50 M/T cells and the olfactory nerves that innervate them form dense regions of neuropil called "glomeruli" (Shepherd, 1998). Molecular biological studies have revealed that sensory neurons in the nasal epithelium express ~1000 types of G-protein coupled odorant receptors (Buck and Axel, 1991) and

individual olfactory sensory neurons express only a single or a few types of these receptors. The axons of olfactory sensory neurons, which express the same odorant receptors, converge selectively to only 1-2 defined glomeruli in the olfactory bulb (Mombaerts et al., 1996; Vassar et al., 1994). Individual M/T cells project a single primary dendrite to a single glomerulus. Thus, an individual glomerulus and its contingent of M/T cells is thought to be a functional unit ("module") representing a single type (or a few types) of odorant receptor (Fig. I.2).

In addition to receiving sensory inputs from the olfactory epithelium, neurons in the OB also receive dense feedback excitatory projections from olfactory cortical pyramidal cells (de Olmos et al., 1978; Haberly and Price, 1978a, b; Luskin and Price, 1983b). These centrifugal fibers terminate in the granule cell layer of the OB, potentially recruiting granule cells to provide inhibition onto M/T cells (Nakashima et al., 1978). Granule cells are a major source of inhibition in the OB (Fig. I.2). Inhibition from granule cells is proposed to mediate a sharpening of M/T response properties (Balu et al., 2007; Strowbridge, 2009) contributing to odor-discrimination in behaving animals (Abraham et al., 2010).

The anatomical structure of the olfactory bulb has led to the hypothesis that olfactory information is encoded by a chemotopic spatial map of glomerular (and M/T cell) activity in the olfactory bulb (Buck, 1996). In addition to the "spatial code", evidence from insects has led to the proposal that evolving temporal patterns of mitral cell activity can contribute to information processing in the olfactory system (Mazor and Laurent, 2005). Regardless of the precise mechanism used for olfactory coding at the level of the olfactory bulb, the output of individual mitral cells, which represent a

particular odorant molecular feature, must undergo a synthetic process to lead to olfactory recognition and discrimination.

Olfactory cortex

The olfactory system is unusual among sensory systems in the brain in that the first stages of information processing bypass the thalamus (Haberly, 1998a). The axons of M/T cells project directly to a number of cortical areas including the olfactory tubercle, anterior olfactory nucleus, entorhinal cortex, prefrontal cortex and the amygdala. The largest olfactory area is called the piriform cortex (primary olfactory cortex), which is a phylogenetically old brain region and part of the paleocortex. The olfactory cortex is generally believed to be a major site where information regarding odorant molecular features is synthesized and integrated (Haberly, 1998a, 2001). This has led to the idea that olfactory percepts are likely to reflect patterns of neuronal activity in olfactory cortex. Consistent with this notion, lesioning piriform cortex in rodents leads to deficits in the learning of odorants and discrimination of complex odors (Staubli et al., 1987; Zhang et al., 1998).

The olfactory cortex has a much simpler laminar architecture than neocortex, having three layers rather than six (Fig. I.2). Layer 1 contains dendrites, fiber systems, and GABAergic interneurons. It is subdivided into a superficial part, layer 1a, which receives dense afferent fibers from the olfactory bulb within the LOT, and a deeper part, layer 1b, which receives recurrent associational (ASSN) inputs from local excitatory pricipal neurons in the olfactory cortex as well as from other cortical regions. Layer 2/3

contains excitatory principal cells with few interneurons. A high density of associational fibers also make synaptic contacts within layers 2/3.

Thus, layer 2/3 pyramidal cells in piriform cortex receive two distinct classes of glutamatergic synapses: one class conveys primary sensory input, while a different set of associational synapses mediate intra- and intercortical signaling. The afferent sensory input from the LOT occurs at synaptic contacts on the distal dendritic tufts of pyramidal cells (Haberly, 1998a). Associational (ASSN) fibers form synaptic contacts on the proximal and basal dendrites of the same pyramidal cells. A number of anatomical and physiological studies indicate that pyramidal cells receive GABAergic input on their dendrites, cell bodies, and axon initial segments (Ekstrand et al., 2001; Haberly, 1983; Haberly et al., 1987; Kanter et al., 1996; Kapur et al., 1997; Kubota and Jones, 1993; Satou et al., 1982, 1983a, b, c; Tseng and Haberly, 1988; Westenbroek et al., 1987). In brain regions like the hippocampus and cerebellum, classic studies by John Eccles (Andersen et al., 1963a; Andersen et al., 1963b, 1964a, b) as well as more recent work (Mittmann et al., 2004; Mittmann et al., 2005; Pouille and Scanziani, 2001, 2004) indicates that these inhibitory circuits have important functional consequences on principal cell activity. These local inhibitory circuits in the cortex are certain to play a major role in governing the output of pyramidal cells and thus directly influence olfactory coding.

Why study cortical representations of odors?

The dynamic balance of sensory-triggered excitatory and inhibitory synaptic inputs determines stimulus-selectivity of cortical neurons. Although much has been

learned about the encoding of odors in the olfactory epithelium and olfactory bulb, relatively little is know about synaptic transmission in the olfactory cortex. Pioneering physiological studies by the labs of Haberly, Aghajanian, Scholfield, and Wilson have provided much of what is currently known about this brain region (Best et al., 2005; Bower and Haberly, 1986; Demir et al., 1998; Gellman and Aghajanian, 1993; Haberly, 2001; Haberly and Bower, 1984; Illig and Haberly, 2003; Johnson et al., 2000; Kanter and Haberly, 1990, 1993; Ketchum and Haberly, 1993a, c; Kuan and Scholfield, 1986; Linster and Hasselmo, 2001; Marek and Aghajanian, 1996; McCabe and Scholfield, 1985; Scholfield, 1978, 1980, 1983; Sheldon and Aghajanian, 1990, 1991; Wilson, 1998a, b, 2000, 2003). For the most part, these studies relied on extracellular field recordings or sharp microelectrode recordings of pyramidal cells in brain slices.

Functionally, in contrast to the precise spatial odor map of the olfactory bulb, where mitral cells projecting to a single glomerulus encode for a single molecular odorant feature, *in vivo* studies using extracellular single-unit recording electrodes have typically found that olfactory cortical neurons spike to a wide variety of odors (Duchamp-Viret et al., 1996; Haberly, 1969; Rennaker et al., 2007; Wilson, 2000). In addition, the cortical representation of each odor seems to be distributed across the entire olfactory cortex (Illig and Haberly, 2003; Rennaker et al., 2007; Zou et al., 2001; Zou et al., 2005). These results suggest that axons of mitral cells from different glomeruli can converge onto the same pyramidal cells in piriform cortex. ASSN excitatory synapses onto the same pyramidal cells also provide a source of input that could strongly influence the salience of olfactory afferent input.

Olfaction is a fast and dynamic sensory modality; it is highly developed, and crucial for survival for our model system: rats. Recent studies suggest that the spatial and temporal patterns of M/T cell activity encode the initial representations of olfactory information in the brain (Bathellier et al., 2008; Margrie and Schaefer, 2003; Rinberg et al., 2006; Soucy et al., 2009; Spors and Grinvald, 2002). However, odor perception ultimately requires the integration of M/T cell activity in higher cortical brain regions and the synaptic mechanisms underlying cortical odor representations are unknown. In addition, given the simple laminar structure of the olfactory cortex and the nature of olfactory bulb mitral cell projections, the olfactory cortex provides an excellent system to study cortical processing of sensory information that has been largely unexplored.

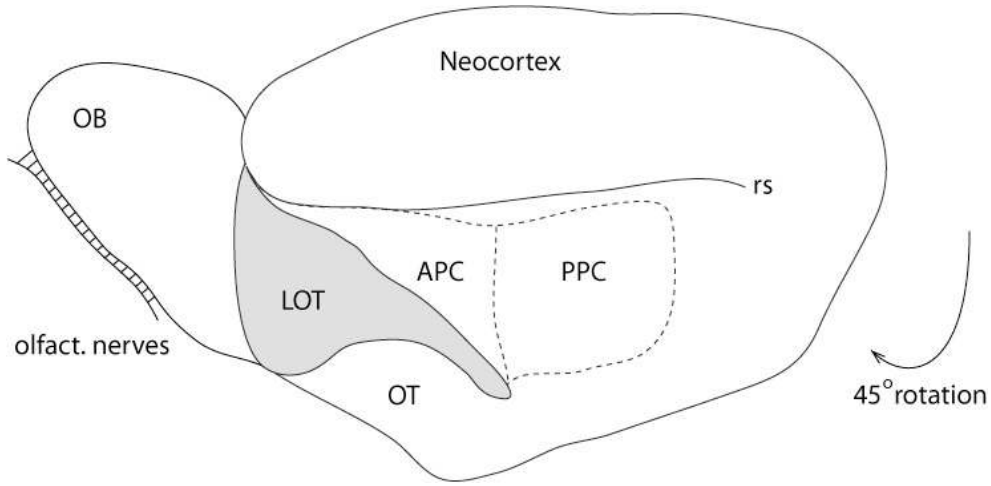

Fig. I.1. Schematic of a rotated rat brain exposing the ventral surface. Olfactory bulb (OB) receives inputs from olfactory sensory neurons (OSNs) located in the nasa epithelium via olfactory nerves. Mitral cells within the OB send their axons via the lateral olfactory tract (LOT) to the anterior piriform cortex (APC) and posterior piriform cortex (PPC). rs: rhinal sulcus. OT: olfactory tubercle.

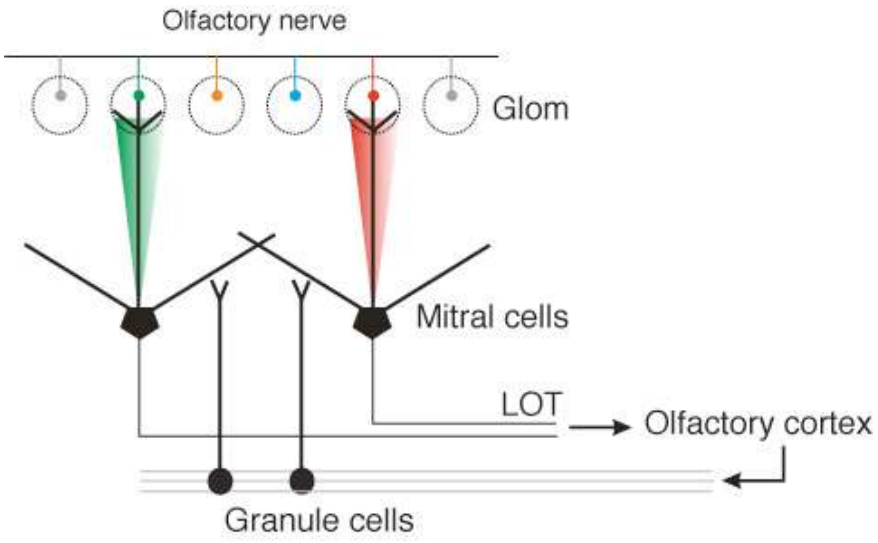

Fig. I.2. Schematic of olfactory bulb. The axons of olfactory sensory neurons, which express the same odorant receptors, converge selectively to the same glomerulus in the olfactory bulb. Individual mitral/tufted cells project a single primary dendrite to a single glomerulus. Granule cells provide local inhibition onto mitral/tufted cells and receive excitatory feedback from pyramidal cells in the olfactory cortex.

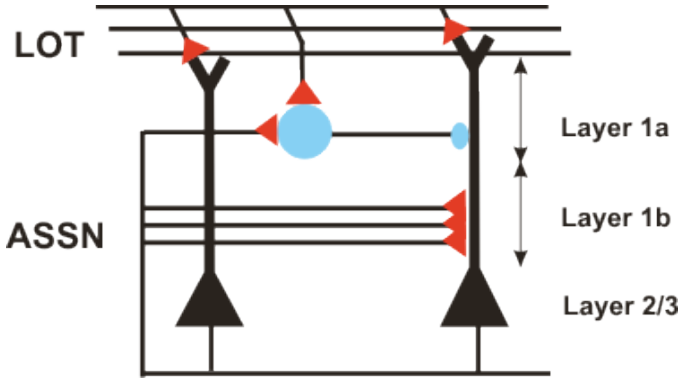

Fig. I.3. Schematic of piriform cortex. Mitral cell axons make up the lateral olfactory tract (LOT) and make excitatory glutamatergic synapses onto the distal apical dendrites of principle pyramidal cells (black). Pyramidal cells (black) are located in layers 2/3. Excitatory glutamatergic synapses also exist between pyramidal neurons, which are terms associational inputs (ASSN). Local inhibitory interneurons (blue) provide inhibitory drive onto principle pyramidal cells are recruited by both mitral cell axons (feedforward inhibition) and pyramidal cell inputs (feedback inhibition).

Experimental Procedures

In vitro electrophysiology

Piriform cortex slices (~400 μm) were prepared from postnatal day 5 (P5) to P35 Sprague Dawley rats in accordance with institutional and national guidelines using standard procedures. Parasagittal cortical slices were cut using a vibrating slicer (Vibratome, St. Louis, MO) in ice-cold artificial CSF (aCSF) containing (in mM) 83 NaCl, 2.5 KCl, 0.5 $CaCl_2$, 3.3 $MgSO_4$, 1 NaH_2PO_4, 26.2 $NaHCO_3$, 22 glucose, and 72 sucrose, equilibrated with 95% O_2/5% CO_2 at 34°C for 30 min and at room temperature thereafter. In the recording chamber, slices were viewed by means of infrared-differential interference contrast (IR-DIC) optics (BX-51W1; Olympus, Tokyo, Japan) and superfused with aCSF containing (in mM) 119 NaCl, 5 KCl, 4 $CaCl_2$, 4 $MgSO_4$, 1 NaH_2PO_4, 26.2 $NaHCO_3$, 22 glucose, and 0.1 picrotoxin, equilibrated with 95% O_2/5% CO_2. The high divalent concentrations (4 mM Ca^{2+} and 4 mM Mg^{2+}) were used to suppress spontaneous epileptiform activity in the presence of the $GABA_A$ receptor antagonist picrotoxin. All experiments were performed at 30–32°C. Baclofen (30 μM) was added to the aCSF to suppress ASSN inputs when isolated LOT inputs were examined (Franks and Isaacson, 2005).

Patch electrodes (3–5 MΩ) contained (in mM) 130 D-gluconic acid, 130 CsOH, 5 NaCl, 10 HEPES, 12 phosphocreatine, 3 MgATP, 0.2 NaGTP, and 0.2 EGTA. Series resistance, which was <15 MΩ, was compensated at 80–95%. The uncorrected liquid junction potential in these recordings was ~12 mV. Synaptic currents were recorded with an Axopatch 200B amplifier (Molecular Devices, Foster City, CA), filtered at 2–5

kHz, collected, and digitized at 10–20 kHz (ITC-18; InstruTech, Mineola, NY). Data acquisition and analysis were performed with Axograph 4.9 (Molecular Devices) and IGOR Pro 4 (Wavemetrics, Lake Oswego, OR) software.

Pyramidal cells for all experiments had cell bodies in deep layer II. Sensory and ASSN EPSCs were evoked using focal stimulating electrodes (1 MΩ pipettes filled with aCSF) placed in the LOT or layer II/III, respectively. Stimulating electrodes were positioned ~150 μm laterally from the recorded cell. The amplitudes of EPSCs were measured over a 0.5–1 ms window centered at the peak of the response. Stimulus strength was set such that EPSCs were 100–200 pA in amplitude under baseline conditions. For the "pairing" protocol, a 5 min baseline was monitored (V_m = –80 mV) using 0.2 Hz stimulation. The cell was then depolarized to 0 mV, and 40 paired-pulse stimuli [50 ms interstimulus interval (ISI)] were delivered at 0.2 Hz. The membrane potential of the cell was then returned to –80 mV after the pairing procedure, and 0.2 Hz stimulation was continued to monitor EPSC amplitude. Pairing was always performed within 5–7 min of breaking into a cell. The magnitude of LTP was determined from the average amplitude of EPSCs 25–30 min after pairing. Summary results and figures include every experiment in which pairing was performed after a stable baseline response was recorded for 5 min. All results represent mean ± SEM.

Two photon imaging

For experiments examining dendritic spines, Alexa 488 (50 μM) was added to the patch electrode internal solution. Imaging was performed with an Olympus Fluoview 300 system modified for two-photon laser microscopy using a femtosecond

laser (MaiTai; Spectra-Physics, Mountain View, CA) tuned to 800–820 nm. Distal apical dendrite segments were used to quantify spines receiving sensory input. All distal apical dendritic regions were verified under IR-DIC optics to overlap with LOT fibers. We restricted measurements of ASSN spines to regions of basal dendrite and proximal apical dendrite (within ~50–100 μm of the soma depending on age). Image stacks (600x magnification, 512 x 512 pixels, 10–20 frames with 0.5 μm steps) were taken of distal apical dendrites and secondary or tertiary proximal apical and basal dendrites. Image stacks were collapsed onto a *z*-projection using maximal intensities from each frame. All image and data analyses were performed with ImageJ (National Institutes of Health, Bethesda, MD) and IGOR Pro 4 (Wavemetrics) software. Dendritic protrusion densities and lengths were averaged across all dendritic segment images obtained from each cell. On average, two to five dendritic segments from each dendritic compartment were pooled for each cell. All analyses were performed blind to the age of animals and to the dendritic compartments of cells.

Surgical procedure for *in vivo* recordings in olfactory cortex

All animal experiments were performed in strict accordance with the guidelines of the National Institutes of Health and the University of California Institutional Animal Care and Use Committee. Sprague Dawley rats (p16–21) were anesthetized with urethane (1.8 g/kg) supplemented with atropine (0.2 mg/kg). Similar results were found in animals anesthetized with ketamine (n=3 cells, data not shown). Body temperature was maintained at 35–37 °C and animals were head-fixed on a custom stereotaxic fixture. After removing a section of temporomandibular muscle, and the ipsilateral eye,

the lateral olfactory tract (LOT) was visualized through the ventral surface of the skull. A small (~1 mm^2) craniotomy was made lateral to the rhinal sulcus, ~1 mm caudal to the middle cerebral artery, and dorsal to the top edge of the LOT to expose the anterior piriform cortical surface. A larger craniotomy (~5 mm^2) was made when LFPs were simultaneously recorded. For LOT stimulation experiments, an additional craniotomy was made ~1.5 mm anterior to the recording site. Respiration was monitored with a chest mounted piezo-electric strap.

Odor Stimuli

Odors were delivered via a computer-controlled olfactometer with a 1 liter/minute constant flow. Odors were diluted 1:10 in mineral oil, and further diluted with charcoal-filtered air to achieve a 5% saturated vapor (SV) in most experiments unless otherwise noted. Odors were presented ~1 cm from the snout in pseudo-randomized order. Odors were presented for 2 s with 60 s between presentations of individual odors. Odors were: cineole, amyl acetate, R-limonene, phenyl ethylalchol, eugenol, dimethyl pyrzadine, citral, and ethyl butyrate.

In vivo electrophysiology

Cell-attached and whole-cell recordings were made with patch pipettes (5–7 MΩ) filled with (in mM): 130 cesium gluconate, 5 NaCl, 10 HEPES, 0.2 EGTA, 12 phosphocreatine, 3 Mg-ATP, 0.2 Na-GTP (7.25 pH; 290–300 mOsm). For data collected using only cell-attached recordings (n=177 cells), neurons were distinguished from glia or other non-neuronal structures by only considering cases in which at least

one AP was detected over several minutes of recording. EPSCs were recorded at −80 mV, the reversal potential for inhibition set by our internal solution (E_{Cl}=−80 mV). Similarly, IPSCs were recorded at the reversal potential for excitation (~+10 mV). Series resistance for whole-cell recording was ≤30 MΩ and continuously monitored. Cells in which series resistance changed by >10% were excluded. L2/3 or layer 1 cells were targeted based on the z-axis readout of an MP-285 micromanipulator (Sutter). A stimulating electrode (FHC) placed within the LOT was used for LOT-evoked synaptic responses. Local field potentials (LFP) were recorded using a tungsten electrode (FHC) in layer 1a ~0.5 mm anterior to the patch electrode recording site. For experiments with *in vivo* pharmacology, all drugs were diluted in oxygenated ACSF at 35°C and superfused over the cortical surface.

Histology

Biocytin (0.2%) was added to the internal solution for experiments with post-hoc histological reconstruction. Briefly, after electrophysiology recordings, an overdose of urethane was given to the animal, after which the animal was decapitated and the whole brain extracted and fixed in 4% paraformaldehyde in 0.1 M phosphate-buffered saline. The recorded hemisphere was then sectioned into 200μm parasagital slices. To recover biocytin-filled cells in whole-mount, cells were revealed by a DAB reaction with nickel intensification. Slices were dehydrated in alcohols and xylenes and mounted in damar resin. These cells were then manually reconstructed using Neurolucida. Cells were identified as interneurons or pyramidal cells based on the following criteria: all layer 1 cells and L2/3 cells with a bipolar or multipolar dendritic tree were categorized

as interneurons (Neville and Haberly, 2004). Pyramidal cells were identified as L2/3 cells possessing a clear apical dendrite and dendritic tree branching towards the LOT, in addition, cells must have basal dendrites that are confined within layers 2/3 (Neville and Haberly, 2004).

Data acquisition and analysis

Recordings were made with a MultiClamp 700A (Molecular Devices), digitized at 5 kHz (Instrutech), and acquired using AxographX (Axograph). Data were analyzed using custom routines in Matlab (Mathworks). Power and coherence spectra with confidence limits were calculated using multitapered methods (Jarvis and Mitra, 2001) and the Chronux package (NIMH). Cells were included in analysis only if >3 odor presentation trials for APs, EPSCs, and IPSCs were obtained. To determine AP responses to odors, we measured APs during a baseline period (2 s) prior to the odor application and during the 2 s odor presentations. Spikes were counted in 200 ms bins. Given the low firing rates of L2/3 cells, we used a combination of two criteria to determine evoked spike activity: 1) average firing rate threshold and 2) spike reliability. Cell-odor pairs needed to satisfy both criteria in order to be categorized as "responsive". For cells that had spontaneous APs: 1) Average firing rate threshold: The average firing rate during the 2 s odor presentation needed to exceed the mean baseline rate + 2.5 standard deviations (S.D.) for ≥3 bins. 2) The firing rate in >50% of trails during odor presentation needed to exceed mean baseline firing rate + 2.5 S.D. in ≥1bin. We chose a threshold of 2.5 S.D. based on a simple receiver-operating characteristic (ROC) analysis (Fantana et al., 2008). Varying the threshold (in terms of mean firing rate + X S.D.)

demonstrated that a threshold of 2.5 S.D. produces a true positive to false positive ratio of 93% (n=177 cells). Thus, we were confident that our method was appropriate for sensitively detecting odor-evoked responses.

For cells with no spontaneous APs: 1) Average firing rate threshold: The average firing rate during the 2s odor presentation needed to exceed 0.5 Hz. 2) The firing rate in >50% of trails during odor presentations needed to exceed 0.5 Hz. The median spontaneous rate was 0.28 Hz, thus, 0.5 Hz was a conservative threshold. We find that varying this threshold from 0.25 to 1 Hz did not alter the number of responsive cell-odor pairs.

Average odor-evoked spiking activity and synaptic currents were aligned to the first inhalation cycle in the presence of odor. Odor-evoked synaptic activity was measured by calculating the charge transfer (Q_{Odor}) during the 2 s odor presentation. Baseline response ($Q_{Baseline}$) was calculated from a 2 s period preceding odor onset. The criteria for a "positive" odor-evoked synaptic response was defined as Response Index (RI)=($Q_{Odor}/Q_{Baseline}$) $\geq$1.6. This threshold value was also derived from ROC analysis of varying RI thresholds to obtain the optimal threshold producing a true positive to false positive ratio of >90% (Fig. 2.2).

To eliminate ambiguity inherent to binary classification of odor-cell pairs as responsive or nonresponsive, we used an additional selectivity measurement: lifetime sparseness (S_L; (Rolls and Tovee, 1995; Willmore and Tolhurst, 2001), which is independent of detection threshold. In brief, S_L was calculated as $(1 - \{[S^N_j\, r_j/N]^2/\{S^N_j\, [r_j^2/N]\}\})/(1 - 1/N)$, where r_j was the response of the neuron to odorant j (mean firing rate or charge transfer during odor presentation), and N was the total number of odors.

This provides a measure of how much the response of a neuron was attributable entirely to one odor (highly selective, S_L=1) versus equally distributed across all odors (S_L=0). Population sparseness (S_p) was calculated with the same method, however, r_j was the response of cell j to a single odor, and N was the total number of cells tested with this odor. In this case, S_p provides a measure of how much of the total population response was attributed entirely to one cell (highly sparse, S_p=1) versus equally distributed across all cells (S_p=0).

Beta oscillations were detected by digitally filtering the LFP between 8–30 Hz, which did not result in any phase shift, as confirmed by comparing beta troughs in filtered and raw traces. The oscillation cycle amplitude was defined as the peak-to-trough amplitude i.e. the difference between the peaks of a given cycle to the subsequent trough of the same cycle. Events with amplitudes ≥4 S.D. from the mean were detected. The peri-oscillation time histogram (POTH) for spikes and oscillation-triggered average for synaptic currents were determined using a method similar to spike-triggered averaging. In this case, however, the average was triggered by the trough of an oscillation cycle recorded in the LFP. Rayleigh test of non-uniformity was used for the POTH in each cell to evaluate significance of AP-LFP phase coupling. The POTH was fitted with a local linear regression (Chronux) in order to extract the peak firing time during an LFP oscillation cycle.

The phase-lag between EPSC and IPSC for each cell was accessed in two ways: time lag between the oscillation-triggered EPSC and IPSC transformed into phase as well as the phase lag between LFP-EPSC and LFP-IPSC at peak coherence. Both methods yielded identical results. Summary data and error bars are presented as

mean±sem and statistical analysis was performed with paired t-tests unless otherwise noted.

Viral injections

All animal experiments were performed in strict accordance with the guidelines of the National Institutes of Health and the University of California Institutional Animal Care and Use Committee. Mouse pups from crosses of Ntsr1-cre heterozygotes and ICR WT mice were injected at p0-2 since the skull at this age is soft enough to be penetrated by an injection pipette. Pups were isoflurane-anesthetized and positioned in a custom-made mold. Injections were targeted to the anterior piriform cortex based on empirically determined landmarks including the posterior border of the eye and the superficial temporal vein. Injections (13.6 nl) of High-titer ($1.2^{*}10^{12}$) stock of AAV2/8-DiO-FLOX-eNPHr3.0-YFP were made using a Nanoject II injector (Drummond Scientific) fitted with a pulled glass beveled micropipette. Location and depth were controlled using a three-axis micromanipulator. Anterior piriform cortex was injected at a depth of (0.25–0.5 mm) and the pipette was kept at each site for 30 s to allow virus to spread locally.

Transgenic mice

Ntsr1-cre animals (Tg(Ntsr1-cre)209Gsat) were obtained from the Gensat Project and the full expression pattern of Cre-recombinase in this line can be viewed at http://www.gensat.org/creGeneView.jsp?founder_id = 44880&gene_id = 511. Ntsr1-cre mice were crossed with the Rosa-YFP reporter line (*Gt(ROSA)26Sor*$^{tm1(Smo/\ (EYFP)Cos}$/J,

Jackson Laboratory) to produce mice expressing YFP in pyramidal cells of piriform cortex.

Photostimulation

For in vitro slice recordings, light from a 598 nm LED (Thorlabs) was collimated and delivered via the 40× objective. Objective was positioned over L2/3 for olfactory cortex pyramidal cell recordings, and over granule cell layer for olfactory bulb granule cell recordings. For in vivo recordings, 1mm fiber-coupled LED (592nm Doric Lenses, 8mW) driven by LED driver (Thorlabs) is used. LED fiber is placed directly over the craniotomy at ~1mm distance from the surface of the brain.

Chapter 1. An early critical period for long-term plasticity and structural modification of sensory synapses in olfactory cortex

Abstract

Critical periods for plasticity of thalamic sensory inputs play an important role in developing neocortical circuits. During an early postnatal time window, pyramidal cells of visual, auditory, and somatosensory cortex undergo structural refinement and possess an enhanced ability for activity-dependent synaptic plasticity. In olfactory cortex, however, pyramidal cells receive direct sensory input from the olfactory bulb, and it is unclear whether the development of olfactory sensory circuits is governed by a critical period. Here, we show that NMDA receptor-dependent long-term potentiation and dendritic spine maturation occur only during a brief postnatal time window at sensory synapses of olfactory cortex pyramidal cells. In contrast, associational synapses onto the same cells retain the capacity for plasticity into adulthood.

Introduction

In the visual, auditory, and somatosensory systems, sensory experience modifies cortical circuits during a short, postnatal "critical period" after which synaptic reorganization is difficult to induce (Hensch, 2004; Katz and Shatz, 1996). However, little is known about the mechanisms governing the early development and plasticity of olfactory circuits.

Olfactory sensory information is conveyed from olfactory receptor neurons (ORNs) in the nasal epithelium to the olfactory bulb. Here, ORNs expressing unique types of odorant receptors project to stereotyped subsets of principal mitral cells, which are thought to represent a spatial map of odor information (Mombaerts, 2001; Ressler et al., 1994) . However, the coding of odor quality and olfactory perception itself ultimately involves the activity of neurons in higher brain regions.

Primary olfactory (piriform) cortex is a major cortical region believed to play an important role in the representation of olfactory information (Haberly, 1998b). Axons of olfactory bulb mitral cells coalesce in the lateral olfactory tract (LOT) and make dense connections with pyramidal cells of the anterior piriform cortex. This afferent sensory input targets the distal apical dendrites of layer 2/3 (L2/3) pyramidal cells (Price, 1973), whereas associational (ASSN) fibers from various cortical regions target proximal apical and basal dendrites (Haberly and Presto, 1986; ul Quraish et al., 2004). Given the precise mapping of particular odor features onto mitral cells, it may be that LOT sensory synapses in olfactory cortex are "hardwired" for the coding of olfactory information. For example, to maintain an invariant representation of specific odor features, activity-dependent plasticity of LOT inputs may not necessarily be desirable. Consistent with

this notion, previous studies of LOT-evoked field EPSPs (fEPSPs) in adult rat olfactory cortex slices found that NMDA receptor (NMDAR)-mediated long-term potentiation (LTP) was not reliably induced by tetanic stimulation (Jung et al., 1990). Successful LTP induction was difficult to achieve and resulted in only modest (10–15%) increases in synaptic strength (Jung et al., 1990; Kanter and Haberly, 1990, 1993). However, given that NMDARs contribute more to LOT transmission in neonatal cortex (Franks and Isaacson, 2005), sensory synapses in piriform cortex may have an enhanced capacity for plasticity during early postnatal development.

Newborn animals (including humans) use olfactory information to form strong maternal attachments, and this "imprinting" to maternal odors is crucial for survival in many species (Leon, 1992; Sullivan, 2003). This strong behavioral plasticity is limited to neonatal animals. These findings imply that in addition to being both functional and necessary at birth, central olfactory circuits could display enhanced plasticity during the early postnatal stage. However, it is unknown if the plasticity and maturation of synaptic transmission in the olfactory cortex could underlie this developmental time window for imprinting.

In this study, we examine whether a critical period for synaptic plasticity and structural development may occur in olfactory cortex. We use whole-cell recording to investigate NMDAR-dependent LTP at sensory LOT inputs and ASSN synapses onto the same pyramidal cells. We find that LOT inputs express robust LTP in neonatal animals; however, the magnitude of LTP at this sensory synapse declines rapidly during the first month of postnatal development. In contrast, the capacity of ASSN inputs to express robust NMDAR-dependent LTP remains throughout adulthood. In addition, we

also characterize the maturation of dendritic spines in pyramidal cell dendritic regions primarily devoted to LOT or ASSN synapses. We find a more rapid maturation of dendritic spines at the site of LOT input compared with ASSN synapses. Together, these results suggest a developmental critical period for the plasticity of olfactory sensory inputs in piriform cortex.

Results

NMDAR-dependent LTP of sensory and ASSN synapses in olfactory cortex

Previous reports of activity-dependent plasticity at sensory synapses in olfactory cortex monitored the effect of theta-burst or tetanic stimulation on LOT-evoked extracellular fEPSPs (Jung et al., 1990; Kanter and Haberly, 1990, 1993; Stripling et al., 1991). We used whole-cell recording to study LOT-evoked EPSCs recorded from layer II pyramidal cells in rat anterior piriform cortex slices (Franks and Isaacson, 2005; Jung et al., 1990; Kanter and Haberly, 1990). In newborn rats (P5–P10), we alternately stimulated two independent LOT inputs (each input at 0.2 Hz) onto a single voltage-clamped pyramidal cell (V_m = –80 mV) (Fig. 1.1A_1). Glass focal stimulating electrodes were positioned in the LOT and bracketed the recorded pyramidal cell with a spacing of ~100 μm. The independence of the two LOT pathways was always confirmed by verifying that simultaneous stimulation of the two pathways produced an EPSC in the pyramidal cell that was the algebraic sum of the EPSCs produced by stimulation of each pathway alone.

To investigate NMDAR-dependent LTP, we used a pairing protocol (see Materials and Methods), the goal of which is to "pair" presynaptic stimulation with

postsynaptic depolarization. After a baseline period of 5 min, the neuron was depolarized to 0 mV to remove the voltage-dependent Mg^{2+} block of NMDARs. During this depolarization, only one of the two pathways (the "paired" pathway) was stimulated. The other pathway ("unpaired") thus served as control for the depolarization alone. This produced an LTP of EPSCs (78 ± 11%; $n = 9$; range, 46–134%) in the paired pathway, whereas the EPSCs of the unpaired pathway were unaffected (Fig. 1.1A_2). This pairing-induced LTP demonstrates that synapse specific plasticity at sensory LOT synapses does not require widespread activation of fibers through tetanic stimulation.

Previous studies of LOT-evoked field potentials demonstrated that LTP induced by theta-burst stimulation is blocked by the NMDAR antagonist APV (Jung et al., 1990; Kanter and Haberly, 1990). To confirm the role of NMDARs in pairing-induced LOT LTP, in a subsequent set of experiments, we interleaved pairing of a single pathway in control slices (80 ± 3%; $n = 5$; range, 30–126%) with slices maintained in the presence of APV (100 μM; $n = 5$). In the presence of APV, pairing-induced LTP was abolished (Fig. 1.1A_3) (Student's t test, $p < 0.05$). In a subset of experiments (Fig. 1.1A_2, A_3), we used paired-pulse stimulation (50 ms, ISI) to monitor presynaptic function during LTP. LOT synapses showed paired-pulse facilitation (EPSC2/EPSC1), which was unchanged during LTP (Fig. 1.1A_4) (paired Student's t test, $p = 0.90$), consistent with a postsynaptic locus for LTP expression (Nicoll and Malenka, 1999). Together, these results show that synapse-specific, NMDAR-dependent LTP can be triggered at olfactory sensory inputs of newborn rats.

In contrast to neonatal rats, we found that plasticity of sensory synapses was markedly reduced in animals that were slightly older (P15–P19). In these experiments,

we monitored the strength of LOT and ASSN inputs onto the same pyramidal cells (Fig. 1.1B_1) and paired stimulation with membrane depolarization in both pathways. Compared with the P5–P10 age group, the amount of LTP induced at LOT synapses was drastically reduced (26 ± 11%; n = 7; range, 9–62%). In these same cells, ASSN synapses potentiated strongly (91 ± 13%; n = 7; range, 72–188%) (Fig. 1.1B_2) (n = 7). Increasing the number of EPSCs paired with depolarization did not lead to greater LTP at LOT synapses (data not shown), indicating that our pairing procedure yielded the maximal amount of potentiation. Interleaving control slices with those in the presence of APV (n = 5 and 8, respectively) revealed that LTP of ASSN synapses required activation of NMDARs (Fig. 1.1B_3) (Student's t test, $p < 0.05$). Under our conditions, ASSN synapses show weak paired-pulse depression at an ISI of 50 ms, and there was no change in the ASSN paired-pulse ratio after induction of LTP (Fig. 1.1B_4) (paired Student's t test, $p = 0.79$). Thus, like LOT inputs, ASSN synapses also exhibit pairing-induced postsynaptic expression of NMDAR-dependent LTP.

We recorded from olfactory pyramidal cells throughout the first month of postnatal life and found a significant decrease in the amount of LTP expressed at sensory synapses by the second postnatal week (Fig. 1.2). A consistent decrease in the amount of LTP expressed at LOT synapses was observed at later developmental time points. By the fourth postnatal week, LOT synapses failed to express any long-term plasticity. In sharp contrast, robust LTP could be elicited at ASSN synapses of the same pyramidal cells throughout this developmental time window, with no obvious difference in the magnitude of potentiation at any time point. We performed regression analysis on the two data groups to determine the differences in correlation of LTP amplitude versus

age. For LOT synapses, a linear regression yielded $R^2 = 0.92$, with a correlation coefficient p value of 0.0091, whereas for ASSN synapses, $R^2 = 0.19$ and the correlation coefficient p value is 0.56. Thus, although there is a strong correlation between age and LTP at LOT synapses, there is no significant correlation at ASSN synapses.

Developmental maturation of spine density occurs rapidly at LOT input sites

We next considered the developmental profile of spine density in dendritic compartments devoted to LOT and ASSN synapses. To rule out the possibility that intrinsic differences between apical and basal dendrites could govern the development of spine density, we imaged proximal apical dendrites in addition to distal apical and basal dendrites in a subsequent series of experiments ($n = 8721$ spines from 48 cells). Consistent with observations in other cortical areas (Whitford et al., 2002), we observed a significant increase in spine density of apical and basal dendritic compartments during development (Fig. 1.2A_2). However, the pooled data from all cells (Fig. 1.2B) indicated that spne density reached mature levels earlier at the site of LOT input (distal apical dendrites; exponential time constant of 3 d) versus compartments devoted to ASSN input (basal and proximal apical dendrites; exponential time constants of 12 and 16 d, respectively). Thus, as for synaptic plasticity, there is a brief developmental time window during which dendritic regions primarily devoted to sensory input undergo structural modification.

Discussion

In this study, we examined NMDAR-dependent plasticity and the structural maturation of sensory synapses in primary olfactory cortex. Our results indicate that during early development, sensory and ASSN synapses onto the same olfactory cortical pyramidal cells differ in their capacity for plasticity and spinogenesis.

Previous studies have established that NMDAR-dependent LTP is an important property of ASSN synapses in piriform cortex (Kanter and Haberly, 1990, 1993). Indeed, it has been suggested that activity-dependent plasticity of ASSN inputs could enhance the salience of odor-evoked responses in pyramidal cells and contribute to olfactory learning in adults (Lebel et al., 2006; Quinlan et al., 2004). However, a role for activity-dependent plasticity at the sensory afferent LOT synapses of olfactory cortex pyramidal cells is less clear. Although it has often been suggested that LOT synapses can express NMDAR-dependent plasticity, several studies in adult rats using a range of tetanic stimulus protocols have shown only a modest and somewhat unreliable potentiation of LOT-evoked fEPSPs after tetanic stimulation (Jung et al., 1990; Kanter and Haberly, 1990, 1993; Stripling et al., 1991).

Our results using intracellular recording and pairing of stimulation with depolarization indicate that strong NMDAR-dependent LTP of LOT synapses occurs during a brief postnatal period, after which there is a decrease in the ability of LOT synapses to undergo potentiation with our pairing protocol. The gradual decline in pairing-induced LTP at LOT inputs is consistent with previous results indicating a marked developmental downregulation of NMDARs at sensory but not ASSN inputs (Franks and Isaacson, 2005). We believe that the rapid developmental loss of NMDARs at LOT synapses can explain why previous fEPSP studies in adult animals reported

relatively unreliable and modest LTP. In contrast, the large, developmentally stable NMDAR component of synaptic transmission at ASSN synapses (Franks and Isaacson, 2005) would permit expression of synaptic plasticity in this pathway throughout adulthood.

We also observe marked differences in the structural maturation of dendritic compartments primarily devoted to LOT (distal apical dendrites) and ASSN (basal and proximal apical dendrites) input. Although we cannot rule out that some of the distal apical dendritic branches may receive ASSN inputs, these most distal branches undoubtedly receive predominantly LOT inputs. Basal dendrites, on the other hand, are solely targeted by ASSN. Although spine density increased during the first few postnatal weeks in both compartments, distal apical dendrites reached a plateau in spine density much earlier than basal dendritic regions. Proximal apical dendrites, which also receive ASSN input, showed a slow time course for spine density development that was quite similar to basal dendrites. Indeed, the maturation of LOT spine density is nearly complete by P9. This rate of maturation appears to be more rapid than other regions of sensory cortex where spine density increases dramatically beyond P9 (Micheva and Beaulieu, 1996; Miller and Peters, 1981). It may be that this early maturation of sensory dendritic regions in piriform cortex is associated with olfaction being completely functional in rodents at birth.

It is possible that the experience-dependent downregulation of NMDARs at sensory LOT synapses (Franks and Isaacson, 2005) could underlie both the critical period for LTP as well as the early maturation of dendritic spine density. For example, in addition to mediating activity-dependent plasticity, NMDARs are also thought to play

a role in the development of dendritic spines (Lin et al., 2004; Tada and Sheng, 2006; Tolias et al., 2005). Studies have also shown *de novo* dendritic spinogenesis associated with NMDAR-dependent synaptic plasticity (Engert and Bonhoeffer, 1999; Maletic-Savatic et al., 1999). Thus, although the developmental time courses over which LTP at LOT inputs declines and spine density matures do not overlap completely, the similarities in their time courses suggest the possibility of a common underlying mechanism. Furthermore, even assuming a common underlying mechanism, divergent mechanisms for LTP expression and spinogenesis would most likely produce differences in the developmental profile of the two phenomena. An alternative possibility that we cannot exclude is that these observations arise from entirely independent mechanisms.

Together, the physiological and anatomical features of developing LOT synapses provide strong support for the notion that there is a critical period for the modification of olfactory input to the cortex. Our results are consistent with reports of critical periods for anatomical and synaptic plasticity in the visual (WIESEL and HUBEL, 1963), somatosensory (Woolsey and Wann, 1976), and auditory cortices (Zhang et al., 2001). The plasticity of developing olfactory sensory inputs could provide a substrate for enhancing the cortical representation of odors experienced during an early postnatal time window. The loss of activity-dependent LTP and the rapid maturation of the dendritic compartment targeted by LOT inputs suggest that there is a "hardwiring" of sensory synapses early in life. In contrast, the persistence of plasticity at ASSN synapses provides a basis for modifying the salience of odor information represented by pyramidal cells throughout adulthood.

Fig. 1.1 NMDAR-dependent LTP of sensory and ASSN synapses. **A**, Synaptic plasticity of LOT synapses in P5–P10 rats. $\mathbf{A_1}$, Recording configuration. $\mathbf{A_2}$, Pairing stimulation of one LOT pathway with depolarization induces LTP (filled circles), whereas the unpaired pathway (open circles) is unaffected. Traces show EPSCs from one cell before and 30 min after LTP induction at paired (left) and control (right) inputs. $\mathbf{A_3}$, APV prevents the induction of LTP at LOT synapses (open circles), whereas interleaved control recordings (filled circles) show robust LTP. $\mathbf{A_4}$, LTP of LOT synapses in $\mathbf{A_2}$ and $\mathbf{A_3}$ does not alter the paired-pulse ratio (n = 11). Traces before and 30 min after LTP induction from one cell are superimposed (left) and scaled (right). **B**, Synaptic plasticity of LOT and ASSN synapses in P15–P19 rats. $\mathbf{B_1}$, Recording configuration. $\mathbf{B_2}$, Pairing both LOT and ASSN inputs elicits robust LTP at ASSN synapses (open circles) and weak LTP at LOT synapses (filled circles). $\mathbf{B_3}$, APV blocks LTP induction at ASSN synapses. $\mathbf{B_4}$, LTP of ASSN synapses in $\mathbf{B_2}$ is not accompanied by a persistent change in the paired-pulse ratio (n = 5). Calibration: 5 ms, 100 pA. Rec, Recording; Pre, before; Post, after.

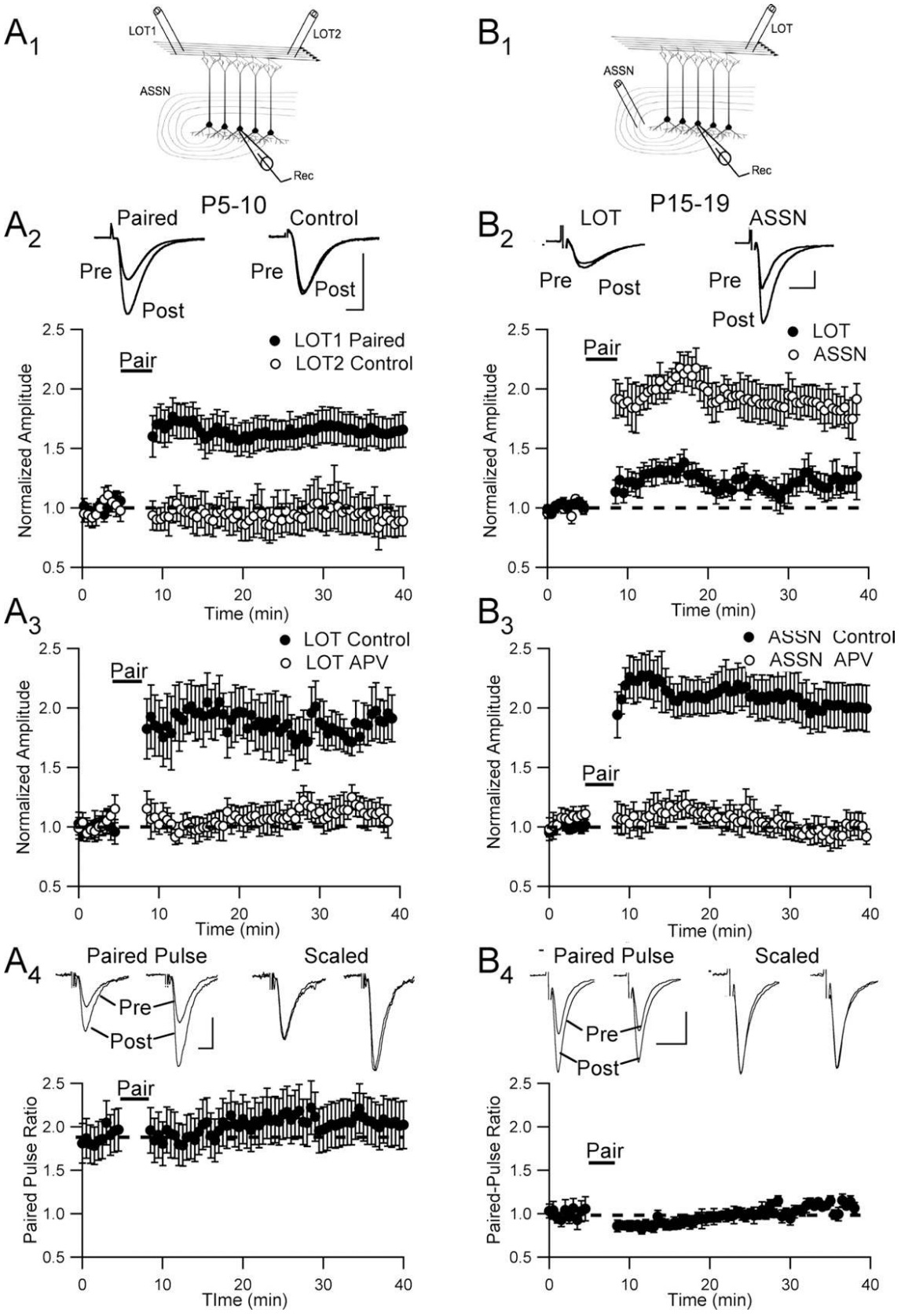
A1
LOT1
LOT2
ASSN
Rec
P5-10
A2
Paired
Control
Pre
Post
Pre
Post
LOT1 Paired
LOT2 Control
Pair
Normalized Amplitude
Time (min)
A3
LOT Control
LOT APV
Pair
Normalized Amplitude
Time (min)
A4
Paired Pulse
Scaled
Pre
Post
Pair
Paired Pulse Ratio
TIme (min)
B1
LOT
ASSN
Rec
P15-19
B2
LOT
ASSN
Pre
Post
Pre
Post
LOT
ASSN
Pair
Normalized Amplitude
Time (min)
B3
ASSN Control
ASSN APV
Pair
Normalized Amplitude
Time (min)
B4
Paired Pulse
Scaled
Pre
Post
Pair
Paired-Pulse Ratio
Time (min)

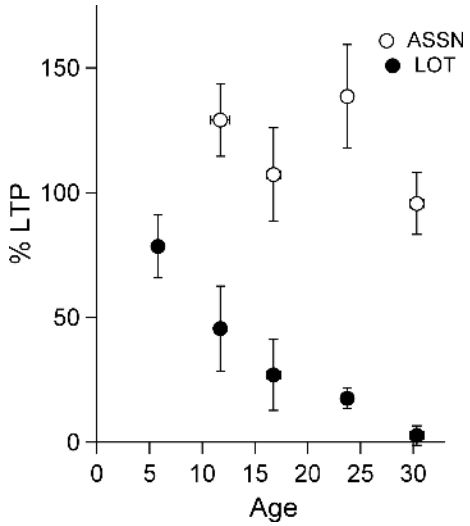

Fig. 1.2 Summary data of LTP at LOT and ASSN synapses during the first postnatal month (n = 3–7 slices per point). The average LOT LTP magnitudes for age groups P5–P10, P11–P14, P15–P19, P20–P26, and P30–P35 were 78 ± 11, 45 ± 17, 26 ± 11, 17 ± 4, and 3 ± 3%, respectively. The average ASSN LTP magnitudes for age groups P11–P14, P15–P19, P20–P26, and P30–P35 were 129 ± 14, 107 ± 18, 138 ± 20, and 95 ± 12%, respectively.

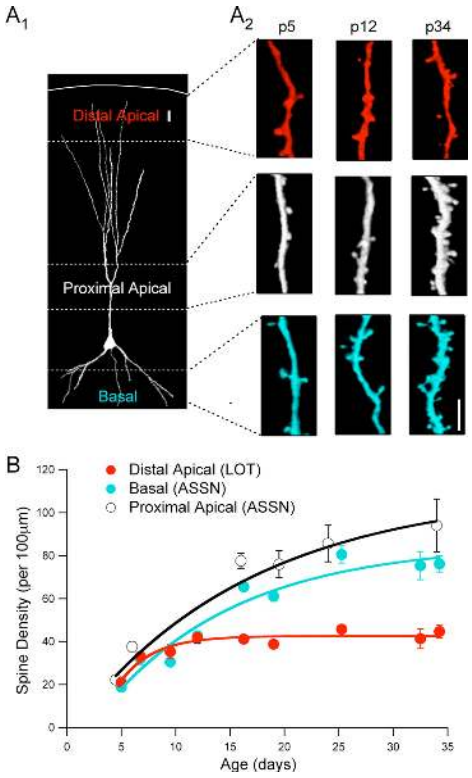

Fig. 1.3 Developmental maturation of spine density at LOT input. **A_1**, Two-photon image of a representative pyramidal cell (P34). Dashed lines indicate boundaries from which distal apical, proximal apical, and basal dendritic spines were measured. The solid line represents pial surface. Scale bar, 20 µm. **A_2**, Distal apical (red), proximal apical (white), and basal dendritic (blue) regions from three cells at age P5, P12, and P34. Scale bar, 5 µm. **B**, Developmental time course for increases in spine density at distal apical, proximal apical, and basal dendritic compartments. Each symbol represents values averages pooled over 2 d intervals. Distal apical spine density data for the nine age groups starting from P5–P6 to P34–P35 are as follows: 21 ± 0.9, 33 ± 1.5, 35 ± 3.3, 42 ± 1.6, 41 ± 0.8, 38 ± 1.0, 46 ± 1.5, 41 ± 4.6, and 45 ± 3.1 spines/100 µm; n = ~12 cells for each age. Basal spine density data for the nine age groups starting from P5–P6 to P34–P35 are as follows: 19 ± 1.3, 32 ± 2.7, 31 ± 1.7, 43 ± 1.7, 65 ± 1.8, 61 ± 2.3, 80 ± 4.0, 75 ± 6.6, and 76 ± 3.8 spines/100 µm; n = ~12 cells for each age. Proximal apical spine density data for the seven age groups starting from P5–P6 to P34–P35 are as follows: 22 ± 1.9, 38 ± 2.2, 41 ± 2.7, 77 ± 3.5, 76 ± 6.3, 86 ± 8.6, and 94 ± 12.3 spines/100 µm; n =5 cells for each time point. Lines are exponential fits with time constants of 3, 12, and 16 d for distal apical, basal, and proximal apical dendrites, respectively.

Acknowledgements

This chapter is a reprint of the material as it appears in Poo C. and Isaacson, J.S. An Early Critical Period for Long-Term Plasticity and Structural Modification of Sensory Synapses in Olfactory Cortex J Neurosci. 2007 July 11; 27(28):7553-7558. The dissertation author was the primary author of this material.

Chapter 2. Odors evoke “sparse” spiking, selective excitation and wide spread inhibition in olfactory cortex

Abstract

The properties of cortical circuits underlying central representations of sensory stimuli are poorly understood. Here we use in vivo cell-attached and whole-cell voltage-clamp recordings to reveal how excitatory and inhibitory synaptic input govern odor representations in rat primary olfactory (piriform) cortex. We show that odors evoke spiking activity that is sparse across the cortical population. We find that unbalanced synaptic excitation and inhibition underlie sparse activity: inhibition is widespread and broadly tuned, while excitation is less common and odor-specific. "Global" inhibition can be explained by local interneurons that receive ubiquitous and nonselective odor-evoked excitation.

Introduction

The functional properties of cortical circuits play a critical role in the central representations of sensory stimuli. However, the synaptic mechanisms governing stimulus-selective spike output in sensory cortices are still debated. Broadly tuned (lateral) inhibition is a fundamental physiological mechanism often proposed to sharpen responses to preferred stimuli, primarily by counteracting weak, nonpreferred excitatory input (Hartline et al., 1956; Priebe and Ferster, 2005). Surprisingly, intracellular studies in visual, auditory, and somatosensory cortex find that synaptic excitation and inhibition are co-tuned to the same stimuli and inhibition elicited by nonpreferred stimuli is often weak (Anderson et al., 2000; Priebe and Ferster, 2005; Wehr and Zador, 2003; Wilent and Contreras, 2005), suggesting that primary sensory cortical circuits lack properties supporting lateral inhibition.

Here, we explore the mechanisms governing odor representations in the anterior piriform cortex, a three-layered cortical region that plays a critical role in odor discrimination, recognition, and memory (Neville and Haberly, 2004; Wilson et al., 2006). Layer 2/3 (L2/3) pyramidal cells in anterior piriform cortex receive direct sensory input from M/T cell axons via the lateral olfactory tract (LOT), excitatory inputs from other cortical neurons and inhibition via local GABAergic circuits (Fig. 2.1; (Neville and Haberly, 2004). Individual L2/3 pyramidal cells are likely to receive converging input from M/T cells belonging to different glomeruli (Franks and Isaacson, 2006). Consistent with this idea, histochemical and extracellular studies suggest that individual odors can activate spatially distributed ensembles of neurons, and individual

neurons may respond to multiple odors (Illig and Haberly, 2003; Litaudon et al., 2003; Rennaker et al., 2007; Wilson et al., 2006).

We use *in vivo* cell-attached and whole-cell recordings to reveal how excitatory and inhibitory synaptic input govern odor representations in L2/3 cells of rat primary olfactory cortex. We show that odor-evoked firing activity is sparse and distributed across the cortical neuron population. We find that unbalanced synaptic excitation and inhibition underlie sparse odor representations. Across the cortical population, odor-evoked inhibition is widespread while excitation is less common. In individual cells, excitation is odor-specific and inhibition is nonselective. We show that this "global" inhibition is likely to arise from local interneurons that receive broadly tuned excitation.

Results

Odor-evoked spikes are sparse in olfactory cortex

We first investigated odor representations *in vivo* using cell-attached recordings of action potentials (APs) from anterior piriform cortex L2/3 neurons in urethane-anesthetized, freely breathing rats (n=59). This recording method provides exceptional isolation of single units and is not biased towards the sampling of active or responsive cells (Hromadka et al., 2008; Margrie et al., 2002). Cell-attached recordings revealed low spontaneous firing rates of L2/3 cells (Fig. 2.1B,C_1; median 0.28 Hz, mean 0.73±0.08 Hz, n=177 cells) and APs were frequently time-locked to the ~2 Hz respiratory rhythm (Fig. 2.2; (Buonviso et al., 2006; Litaudon et al., 2003; Rennaker et al., 2007).

Results from a large set of individually sampled neurons (n=177) were used to infer the distribution of odor-evoked firing activity across the cortical population. In order to determine how individual stimuli are represented by the cortical population, we sampled responses to a small, fixed odor set rather than searching for the optimal stimulus for a particular neuron. We tested four monomolecular odors (5% saturated vapor (SV)) with unique and distinct structures and perceptual qualities: cineole (ether, eucalyptus), amyl acetate (ester, banana), limonene (terpene, citrus), and phenylethyl alcohol (alcohol, floral). For each odor tested in every cell (odor-cell pair), we used both changes in mean firing rate and the reliability of firing across trials to categorize activity as odor-evoked or nonresponsive (see Experimental Procedures). Although we observed clear odor-evoked suppression of APs in some cells (n=9 cells, data not shown), the low spontaneous firing rate precluded accurate classification of inhibitory responses.

We first determined the odor-selectivity of individual cells, as well as the population response to each individual odor. In other words, we tested the number of odors each cell responded to, and the number of cells each odor can activate. For cells with odor-evoked responses (55/177), most (42/55) fired selectively to only one of the four odors (Fig. 2.1C_2). In terms of the population response, each odor evoked activity in ~10% of tested cells (Fig. 2.1C_3), indicating that the different odors elicited spikes in relatively small fractions of the cortical population. Interestingly, despite their structural diversity, each unique odor activated very similar fractions (range 9–11%) of the cortical population.

To better understand the distribution of odor-evoked activity in olfactory cortex, we explored the intensity of stimulus-evoked responses. For responsive odor-cell pairs, the average increase in firing rate during the odor stimulus (2 s) was 2.01±0.04 Hz (Fig. 2.1C_1; range 0.05 to 24.5 Hz; median: 0.83 Hz, n=72 odor-cell pairs). Strong responses were rarely observed: only 19% of responses exceeded 5 Hz and very few (6%) exceeded 10 Hz (Fig. 2.1C_1). Evoked APs were coupled strongly to the respiratory rhythm (Fig. 2.1B, Fig. 2.2) and on average odors evoked only an additional 1.6±0.04 spikes (median: 0.6 AP) above baseline during each respiratory cycle throughout the odor stimulus (Fig. 2.1C_4). Thus, odor responses consisted of weak increases in firing rate in the majority of responsive cells, while a small fraction of neurons fired more strongly.

In addition to quantifying odor-selectivity and the population response in terms of odor-cell pairs that were categorized as odor-evoked or nonresponsive, we also used statistical measures calculated from raw firing rate distributions (Rolls and Tovee, 1995; Willmore and Tolhurst, 2001). This provides a description of odor-evoked activity without relying on binary categorization of responses. Lifetime sparseness (S_L, range 0 to1=highly selective), a measure of how an individual cell responds to multiple stimuli (see Experimental Procedures), indicated that cells responded selectively (S_L mean=0.88±0.002, median =1, n=177 cells). Population sparseness (S_p, range 0 to 1=most sparse), a measure of how an individual stimulus is represented across a population, was also high (mean S_p=0.93, range 0.90–0.96). Taken together, our results indicate that odor representations are sparse in olfactory cortex.

Global inhibition and selective excitation underlie sparse odor representations

What governs the sparse population response of L2/3 cells? To address this question, we used *in vivo* whole-cell recording (Margrie et al., 2002) to examine the synaptic input underlying spike output in an additional set of L2/3 cells (n=52). Following cell-attached recording of APs (Fig. 2.2A), excitatory (EPSCs) and inhibitory postsynaptic currents (IPSCs) were recorded in voltage-clamp mode in each cell (Fig. 2.2B). EPSCs were recorded at −80 mV, the reversal potential for inhibition set by our internal solution (E_{Cl}=−80 mV). Similarly, IPSCs were recorded at the reversal potential for excitation (~+10 mV). In the absence of applied odors, cells received barrages of spontaneous EPSCs (77±12 Hz) and IPSCs (57±10 Hz, n=12 representative cells, data not shown) and odors evoked synaptic currents that were coupled to the respiration cycle (Fig. 2.2; Fig. 2.3B). We first examined synaptic responses categorically and determined responsiveness (the presence or absence of odor-evoked activity) for each odor-cell pair from the increase in charge transfer during odor presentation (see Methods).

We first compared the fractions of cells in this population that responded to the different odors with APs, EPSCs, and IPSCs. Each of the different odors elicited responses in similar fractions of cells (Fig. 2.3C). We estimated population sparseness from the fraction of cells responsive to each odor averaged over all odors. While cells with odor-evoked APs were rarely observed (8.3±0.5% of the population), odor-evoked excitation was more common (22.7±1.5%) and inhibition was remarkably widespread (51.8±2.2%, Fig. 2.3C). Furthermore, S_p calculated from unthresholded synaptic charge measurements during odor presentation indicated that excitatory synaptic responses

(S_p=0.72±0.03) were significantly sparser than inhibition (S_p=0.56±0.02, p=0.006). These results suggest that across the cortical population, ubiquitous odor-evoked inhibition contributes to firing activity that is more sparsely distributed than synaptic excitation.

We further explored whether inhibition contributes to sparse odor-evoked firing activity by blocking fast synaptic inhibition with the $GABA_A$ receptor antagonist gabazine (SR-95531). However, local cortical superfusion of gabazine (20–100 μM) led to epileptic activity evident as ictal bursts (~1 Hz) of spikes in cell-attached recordings (n=10). Once epileptic events began, odor-evoked activity was lost and spikes became decoupled from respiration. Nonetheless, in two experiments we observed a broadening in the odor tuning of firing activity in the presence of gabazine before the cortex became epileptic (under control conditions the two cells fired in response to only one of four odors vs. two and three odors in the presence of drug, data not shown).

We next considered the odor selectivity of synaptic excitation and inhibition in individual cells. Although cells with odor-evoked EPSCs were more common than APs (Fig. 2.3C), EPSCs were selectively evoked by only one out of four odors in the majority of cells (60%, Fig. 2.3D). Strikingly, inhibition was recruited non-selectively; in 66% of cells that received inhibition, it was evoked by three or all four odors (Fig. 2.3D). Together, these findings suggest that inhibition is “global” in olfactory cortex, i.e. odors evoke widespread inhibition across the population and inhibition within an individual cell is broadly tuned to odors.

If inhibition were truly global in olfactory cortex, we would predict that the relative strength of inhibition evoked by different odors would be more uniform than

excitation in individual cells. To address this, we examined the relative strength of excitation and inhibition in all cells that fired APs in response to odors (n=13). Excitation (EPSC charge) elicited by each odor was normalized to the largest odor-evoked excitatory response in each cell. Inhibition (IPSC charge) was normalized similarly. Responses in each cell were then ranked from the odor that produced the weakest excitation to the odor that produced the strongest and averaged across cells (Fig. 2.3E_1). As we hypothesized for global inhibition, the strength of excitatory responses was graded, while the strength of inhibition was uniform across odors (Fig. 2.3E_1).

Differing amounts of excitation and uniform inhibition implies that odors trigger APs based on the strength of excitation rather than odor-specific inhibition. Indeed, odors that elicited APs (preferred odors) also evoked greater excitation (average EPSC charge: 46.5±1.5 pC) than those that failed to produce spikes (nonpreferred odors, 16.9±0.7 pC, p=0.002) in the same cells (Fig. 2.3E_2). In contrast, preferred and nonpreferred odors evoked identical amounts of inhibition (Fig. 2.3E_2; average IPSC charge: 78.6±3.7 pC and 77.3±1.7 pC, respectively, p=0.81). Together, these results suggest that odor-evoked excitation must be strong enough to overcome global inhibition to generate APs in olfactory cortex.

To verify that our observations were not specific to our panel of test odors, we studied an additional set of cells (n=34 cells) using double the number of odors. We observed the same relative relationships in the selectivity (Fig. 2.4A_1) and population responses (Fig. 2.4A_2) of odor-evoked activity, i.e. APs were evoked sparsely and selectively, synaptic excitation was more common but specific, and inhibition was

widespread and most broadly tuned. In a subset of these cells, we also examined the relationship between synaptic excitation and inhibition across a range of odor intensities. We varied odor concentration for cells that responded with excitation to multiple odors at our standard concentration of 5% SV. We found that odors were much more likely to evoke inhibition compared to excitation across a range of concentrations (0.25–10% SV). Reducing odor concentration from 5% to 2% SV led to a loss of excitatory responses to some odors while inhibitory responses to the same odors remained (Fig. 2.4B,C; n=9 cells). Indeed, as odor intensity was reduced further, odor-evoked inhibition could be observed in the absence of excitation (Fig. 2.4C). Furthermore, when normalized to the maximal synaptic responses we recorded at 10% SV, the relative amplitudes (charge) of inhibition at low odor concentrations was greater than excitation (Fig. 2.4D). Thus, inhibition is preferentially recruited across a wide range of odor intensities. Together, these results provide strong evidence that global inhibition is a fundamental property of olfactory cortical circuits.

Odor-evoked spikes become more broadly tuned with inhibition blocked

We propose that this global inhibition contributes to the 'sparse' activity seen in olfactory cortex. In other words, global inhibition could serve to suppress the number of spikes each odor evokes, and also the number of odors a given cell responds to. To test this hypothesis, we recorded odor-evoked action potentials from layer 2/3 cells using the cell-attached method in piriform cortex, while superfusing a selective GABA receptor antagonist, gabazine, onto the cortex. We find that with high concentrations of gabazine superfusing (>20μM), piriform cortex spontaneously generated epileptic form

activity, as reflected by ictal events in the local field potential (LFP) measured in layer 1a (Fig. 2.5A). However, with a low concentration of gabazine (<20uM), we find that neurons become more responsive a panel of test odors (Fig. 2.5$B_{1,2}$).

These experiments suggest that the 'global' inhibition we observe plays a significant role in controlling the excitability of the cortex. More importantly, these experiments demonstrate that inhibitory synaptic transmission contributes to restrict the number of odors each cell responds to. However, one caveat in interpreting these experiments is the difficulty in determining effects of direct inhibitory block on a given neuron, versus network effects resulting for increased excitability in gerneral.

Excitation onto local interneurons is broadly tuned

What accounts for global inhibition in olfactory cortex? One possibility is that, unlike principal cells, the local interneurons underlying inhibition receive widespread and broadly tuned excitation. To address this question, we filled cells with biocytin during whole-cell recording for *post hoc* classification. Interneurons were targeted by recording from cells in layer 1 (Neville and Haberly, 2004). Indeed, synaptic excitation was largely nonselective in morphologically identified interneurons (Fig. 2.6$A_{1,2}$; n=18 cells), while identified pyramidal cells received selective excitation (Fig. 2.6$B_{1,2}$; n=27 cells) similar to results from our larger L2/3 population. On average, individual odors evoked excitation in a greater fraction of interneurons compared to pyramidal cells (Fig. 2.6A_3, B_3; interneurons: 50±3.9%; pyramidal cells: 11±2.3%, p=0.003) and inhibition was recruited similarly in both cell types (p=0.2). These findings suggest that

nonselective odor-evoked excitation of local interneurons could underlie global inhibition.

One mechanism that could lead to broadly tuned excitation onto interneurons is if they receive a higher convergence of olfactory bulb M/T cell inputs than pyramidal cells. We examined this possibility *in vivo* by placing a stimulating electrode in the LOT to directly activate M/T cell axons and recording LOT-evoked responses in L2/3 cells (Fig. 2.7A). At high stimulus intensities, LOT stimulation evoked monosynaptic EPSCs (Fig. 2.7B_1) at a holding potential of −80 mV. We then lowered stimulus strength to reduce the number of recruited axons, such that stimulation failed to evoke EPSCs (Fig. 2.7B_2). Changing the membrane potential to +10 mV revealed LOT-evoked IPSCs at the same stimulus intensity that failed to evoke EPSCs (Fig 3.6B_3). Subsequent application of the glutamate receptor antagonist NBQX (500 μM) to the cortical surface abolished the IPSCs, indicating that they were evoked disynaptically (Fig 3.7B_3). The onset times of IPSCs evoked with this "minimal" stimulation lagged behind monosynaptic EPSCs in the same cells (Fig. 2.7C), further confirming their disynaptic nature (Pouille and Scanziani, 2001). Disynaptic IPSCs could routinely be recruited in the absence of LOT-evoked EPSCs (Fig. 2.7D, n=5). These experiments suggest that interneurons governing inhibition in olfactory cortex receive a higher convergence of M/T cell input than pyramidal cells.

Discussion

"Sparse" cortical odor representations

We wished to understand how neuronal populations in olfactory cortex represent individual odors. In other words, what is the typical response of the cortical population to a particular odor? Our approach differs from those that study representations of sensory stimuli by searching for the optimal stimulus for each cell, i.e. to define the "receptive field" of particular neurons. Measuring receptive fields is problematic in olfactory cortex since the number of odors that can potentially be encoded is vast and the topographical mapping of odor space within the cortex is unknown. Here, we used a small, fixed set of odors and data from individually recorded cells to reconstruct the overall population response. This approach allowed us to infer how individual stimuli (odors) are represented across the cortical population. A similar strategy has been used to explore the nature of stimulus representations in the insect olfactory system (Perez-Orive et al., 2002; Szyszka et al., 2005; Turner et al., 2008) and mammalian auditory cortex (Hromadka et al., 2008).

In contrast to extracellular unit recording, cell-attached recordings are not biased toward the detection of neurons with high firing rates. We used this method to sample the distribution of firing rates in olfactory cortex. We find that L2/3 cells *in vivo* have very low spontaneous activity (<1 Hz) and individual odors caused an increase in firing in ~10% of the cortical population. This is consistent with the idea that unique odors are represented by ensembles of active cells and that these cells are distributed similarly across the cortical population.

Given that individual odors can activate 10% of the cortical population, is it valid to describe odor representations as "sparse" in piriform cortex? It is important to bear in mind that the odor-responses of "active" cells were extremely weak. For

responsive cells, odor-evoked increases in firing rate averaged only 2 Hz and only 6% of these cells had “well-driven” responses (>10 Hz). While we tested odors at a moderate concentration of 5% saturated vapor, it is likely that at lower concentrations even fewer cells within the cortical population would be active. Low spontaneous and evoked firing rates have also been reported in other cortical regions from anesthetized and awake animals when activity is measured using patch-clamp recording techniques (Brecht and Sakmann, 2002; DeWeese et al., 2003; Hromadka et al., 2008; Margrie et al., 2002). Together, the low firing rates, the small fraction of the population activated by individual odors, and the rarity of well-driven responses indicate that odor representations are sparse in olfactory cortex (Laurent, 2002; Olshausen and Field, 2004; Rolls and Tovee, 1995; Willmore and Tolhurst, 2001).

It has been reported that responses of olfactory bulb mitral cells to odorants are weaker and less frequently observed in awake behaving animals compared to ketamine/xylazine-anesthetized animals (Rinberg et al., 2006). Thus, odor representations in the olfactory bulb can be sparser in awake animals vs. those in the anesthetized state. While our experiments were performed under urethane anesthesia, a lower level of odor-evoked mitral cell activity may lead to sparser cortical odor representations in the awake, behaving state.

Global inhibition

Extracellular and immunohistological studies suggest that odors can activate ensembles of cells that are spatially dispersed (Illig and Haberly, 2003; Rennaker et al., 2007). The distribution of odor-evoked activity in olfactory cortex is fundamentally

determined by the convergence (Franks and Isaacson, 2006) and divergence of M/T cell axon collaterals (Ojima et al., 1984). Anatomical studies suggest that single M/T cell axons terminate in broad, overlapping patches of olfactory cortex (Buonviso et al., 1991; Ojima et al., 1984). In addition, associative connections between pyramidal cells can amplify and further distribute excitation across the cortical population (Neville and Haberly, 2004; Rennaker et al., 2007). How does the olfactory cortical network counterbalance broadly-distributed afferent excitatory input and highly associative connections to accomplish sparse odor-evoked spiking activity?

We propose that global inhibition is a major feature governing sparse odor representations in olfactory cortex. In contrast to the balanced excitation and inhibition elicited by stimuli in other primary sensory cortices (Anderson et al., 2000; Priebe and Ferster, 2008; Tan et al., 2004; Wehr and Zador, 2003; Wilent and Contreras, 2005), odor-evoked inhibition is widespread and nonselective in olfactory cortex. Global inhibition is poised to dampen odor-evoked excitatory responses across olfactory cortex such that only cells receiving strong and preferred excitation are driven to spike. In addition to promoting sparseness, global inhibition can contribute to cortical odor coding by providing gain control, noise suppression, and state-dependent modulation of cortical activity (Hensch, 2004; Murakami et al., 2005).

We show that global inhibition is likely to reflect the fact that local interneurons receive ubiquitous odor-evoked excitation that is broadly tuned. We suggest that broadly tuned excitation of olfactory cortex interneurons is due to a higher convergence of M/T cell inputs to interneurons than principal cells. In support of this idea, we found that low intensity LOT stimulation consistently evoked disynaptic inhibition in the

absence of excitation in pyramidal cells. While feedforward interneurons in olfactory cortex are likely to play an important role (Luna and Schoppa, 2008)), local feedback circuits may also contribute to global inhibition.

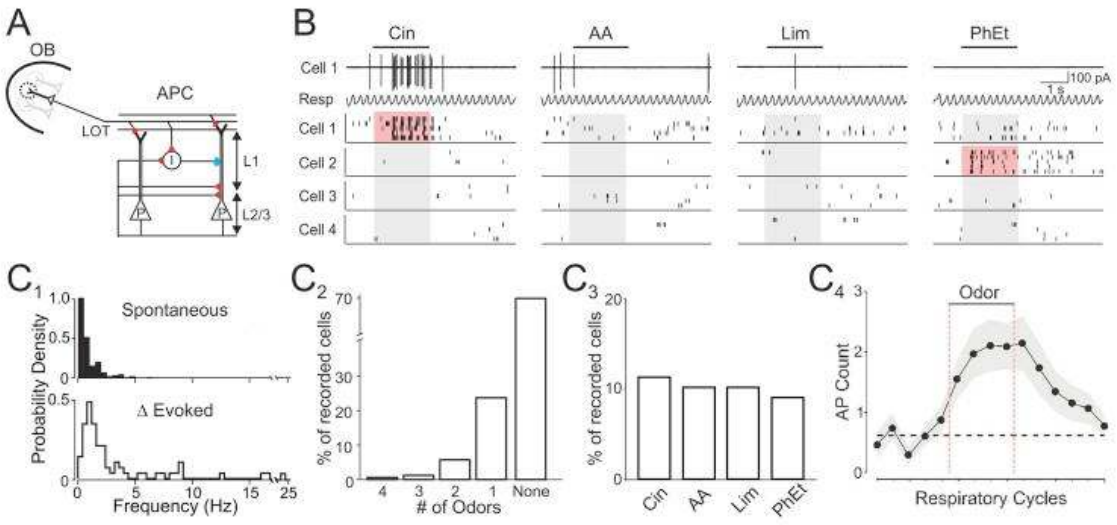

Fig. 2.1 Odor-evoked action potential responses are sparse in olfactory cortex. **A**, Schematic of anterior piriform cortex (APC). Olfactory bulb (OB) M/T cells project axons via the lateral olfactory tract (LOT) onto L2/3 pyramidal cells (P) and local interneurons (I). Red, excitatory and blue, inhibitory synapses. **B**, Raster plots of spikes from four representative cells. Top traces: cell-attached recording of spikes from Cell 1 and simultaneously monitored respiratory rhythm (Resp). Upward deflections in respiration trace correspond to inhalation. Bars indicate odor delivery (2 s) and pink shading indicates evoked responses. **C_1**, Distributions of spontaneous AP frequency (top, n=177 cells) and odor-evoked increases in firing rate (bottom, 72 responsive odor-cell pairs). **C_2**, Distribution of odor selectivity. **C_3**, Population response to individual odors. **C_4**, Mean spike count for each respiratory cycle (n=72 responsive odor-cell pairs). Dashed black line, mean spike count preceding odor delivery. Odors: cineole (Cin), amyl acetate (AA), R-limonene (Lim), phenyl ethylalchol (PhEt).

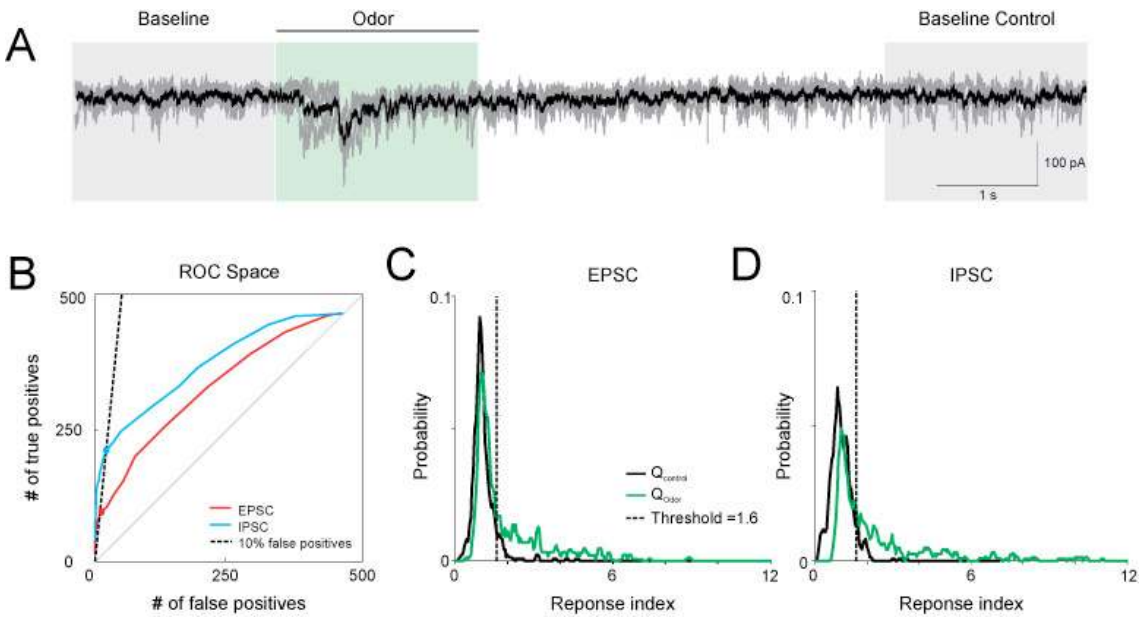

Fig. 2.2 Receiver-Operator Characteristic (ROC) of synaptic currents is used to evaluate odor responses. **A,** Baseline charge ($Q_{Baseline}$) was calculated from the 2 s prior to odor onset. Odor-evoked charge (Q_{Odor}) was calculated over the 2 s odor period. A second control baseline period ($Q_{Control}$) was obtained from the 4–6 s period post odor offset. **B,** For a given threshold, we calculated the number of true positives ($Q_{Odor}/Q_{Baseline}$ > threshold) and false positives ($Q_{Control}/Q_{Baseline}$> threshold). We varied the threshold from 0 to 5. The number of true positives is plotted against the number of false positives for EPSCs (red) and IPSCs (blue) as threshold is varied (n=86 cells). Dashed line: 10% false positive rate. Dots represent points on the ROC curve for EPSC and IPSC at which the false positive rate is 10%. For a 10% false positive rate, threshold was 1.6 and 1.58 for EPSC and IPSC curves, respectively. **C, D,** Probability density of $Q_{Odor}/Q_{Baseline}$ (green) and $Q_{Control}/Q_{Baseline}$ (black) in all odor-cell pairs for EPSCs and IPSCs. Dashed line indicates threshold of 1.6.

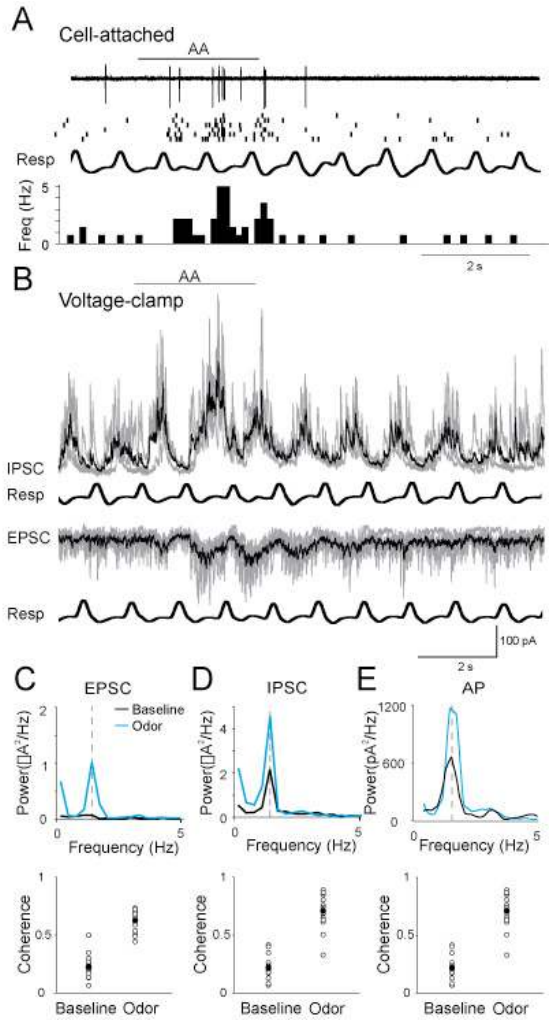

Fig. 2.3 Odor-evoked activity is coupled to respiration. **A, B,** Example recording from a L2/3 cell in cell-attached and whole-cell configuration showing responses to odor (AA, amyl acetate). APs, EPSCs, and IPSCs show respiration-coupled rhythms. Black trace, average current. Grey traces, single trials. **C–E** (top panels), Power spectra of EPSCs, IPSCs and APs for cell in (A) and (B) show peaks at ~2 Hz under baseline conditions (black) that are enhanced in the presence of odor (blue). Grey dashed line indicates the average respiratory rate of this rat (1.7 Hz). **C–E** (bottom panels), Coherence between respiration and EPSCs, IPSCs, and APs during baseline conditions and in the presence of an odor for a population of cells with odor-evoked APs (n=12). Coherence is calculated at the peak of the respiration frequency for each experiment.

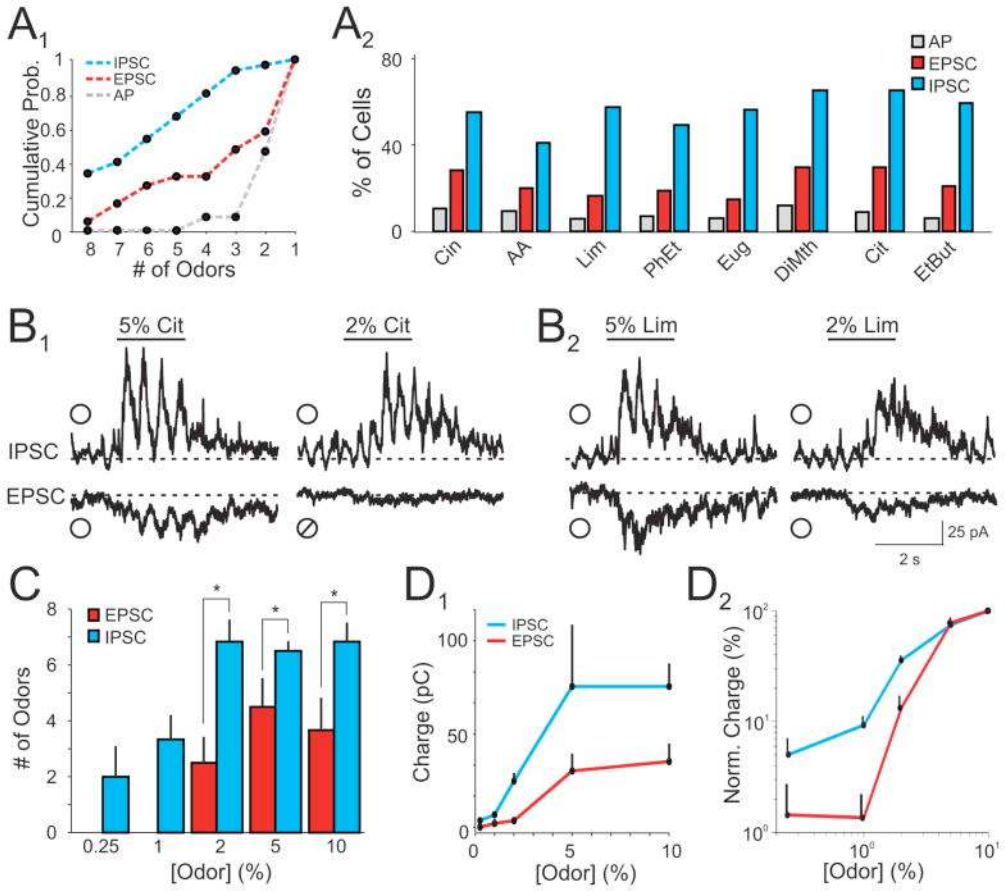

Fig. 2.4 Global inhibition is not dependent on odor identity or concentration. **A_1**, Cumulative probability distribution of odor selectivity for cells tested with eight odors (n=34 cells). **A_2**, Population response of APs, EPSCs, and IPSCs for all cells (n=86 cells). **B**, Representative average EPSCs and IPSCs from a L2/3 cell in response to two odors **B_1, B_2**, at 5% and 2% saturated vapor (SV). ○ indicates a positive odor response, ∅ indicates a negative odor response. **C,** Number of odors that evoked excitation and inhibition in cells tested with eight odors over a range of concentrations. Cells with excitatory responses to multiple odors at 5% SV were selected for these experiments. Each cell was tested with all odors at five concentrations (n=9 cells, * indicate $p<0.05$). **D_1**, Odor-evoked increases in EPSC and IPSC charge across odor concentrations. **D_2**, Normalized odor-evoked charge for EPSCs (red) and IPSCs (blue) plotted on a log-log scale. Odors: cineole (Cin), amyl acetate (AA), R-limonene (Lim), phenyl ethylalcohol (PhEt), eugenol (Eug), dimethyl pyrzadine (DiMth), citral (Cit), and ethyl butyrate (EtBut).

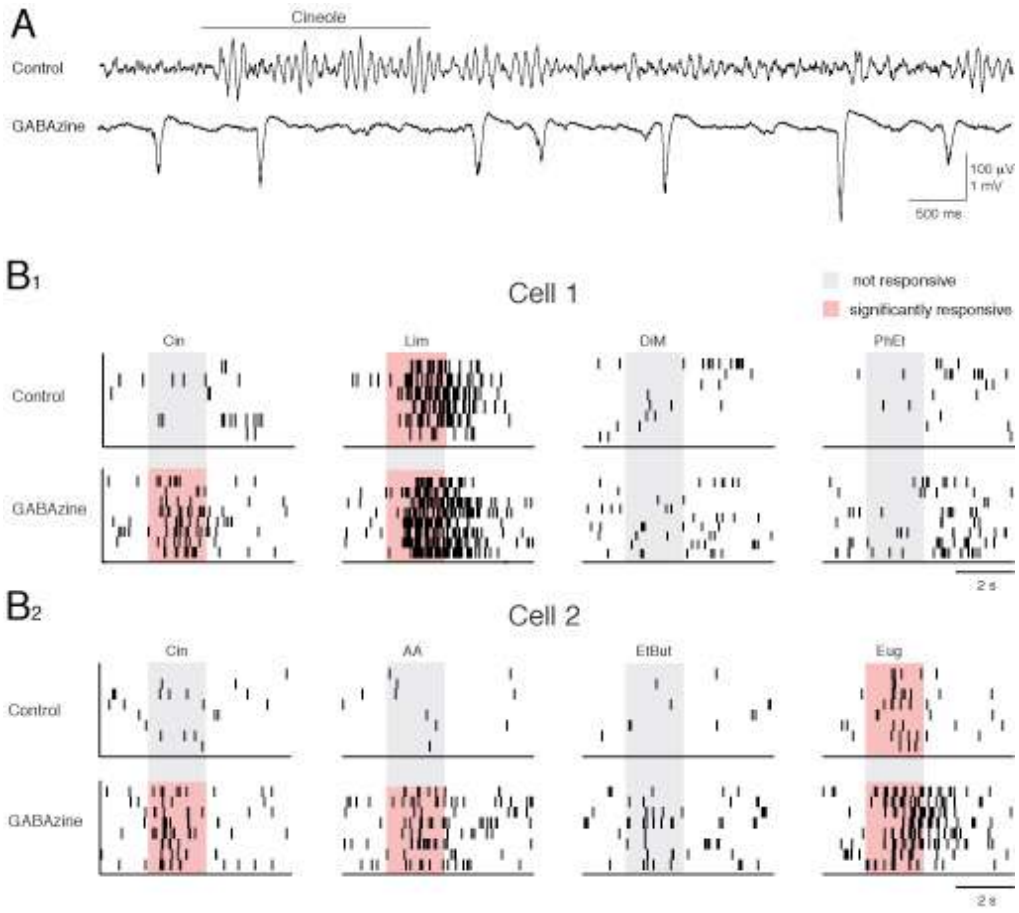

Fig. 2.5 Action potentials of neurons with inhibition blocked. **A**, In contol conditions, odors evoke increased activity in the LFP. 50μM of gabazine superfused on the cortical surface produces large ictal events in the LFP indicative of epileptic-form activity. **B**, Examples of two cells recorded in layers 2/3 with odor-evoked action potentials that become more broadly tuned in the presence of 20μM gabazine. Odors: cineole (Cin), R-limonene (Lim), dimethyl pyrzadine (DiMth), phenyl ethylalcohol (PhEt).

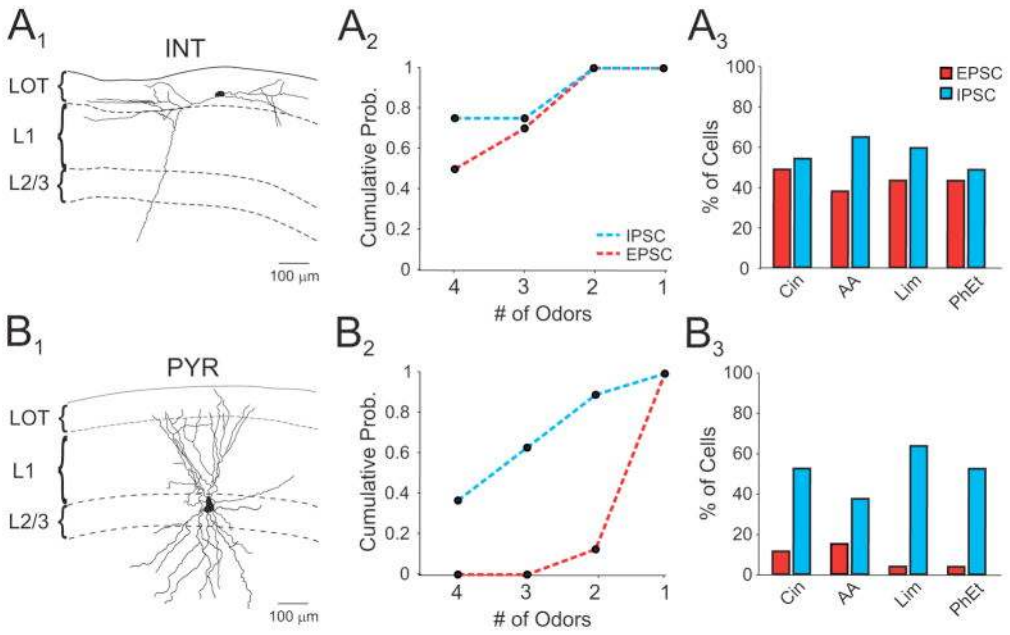

Fig. 2.6 Interneurons receive widespread and broadly tuned excitation. **A_1**, Morphologically identified interneuron following *in vivo* recording. Only the soma and dendritic arbors are shown in reconstruction. **A_2**, Selectivity of odor-evoked EPSCs and IPSCs in interneurons. **A_3**, Interneuron population responses. **B_1**, Morphologically identified pyramidal cell. Only the soma and dendritic arbors are shown in reconstruction. **B_2, B_3**, Pyramidal cell selectivity and population responses. Odors: cineole (Cin), amyl acetate (AA), R-limonene (Lim), phenyl ethylalcohol (PhEt).

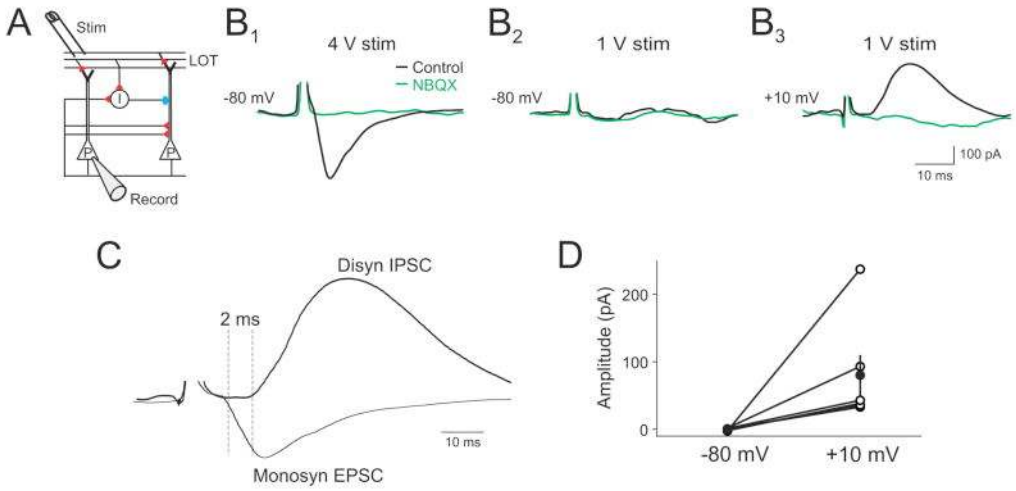

Fig. 2.7 Minimal stimulation of the LOT *in vivo* recruits disynaptic inhibition. **A**, Schematic of recording setup. **B_1**, Under control conditions, direct LOT stimulation evokes a monosynaptic EPSC (V_m=−80 mV) at high stimulation intensity (4 V) in a L2/3 cell. **B_2**, Lowering stimulation intensity (1 V) fails to evoke an EPSC, while depolarization to +10 mV reveals an IPSC. **B_3**, Subsequent application of NBQX (500 μM) to the cortical surface abolishes the monosynaptic EPSC and disynaptic IPSC **$B_{1–3}$** (green traces) and **C**, Overlay of monosynaptic EPSC and disynaptic IPSC. **D**, Summary data of recruitment of disynaptic IPSCs (+10 mV) at stimulus intensities that failed to evoke EPSCs (−80 mV, n=5 cells).

Acknowledgements

This chapter consists of work published in Poo C. and Isaacson, J.S. Odor representations in olfactory cortex: "sparse" coding, global inhibition and oscillations. Neuron. 2009 June 25; 62(6): 850–861. The dissertation author was the primary author of this material.

Chapter 3. Beta (15-30 Hz) frequency oscillatory synaptic inputs govern odor-evoked spike timing in olfactory cortex

Abstract

Recent studies in the olfactory system as well as other sensory cortices suggest that information about the stimulus can be coded not only by a change in neuronal firing rate, but also varying spike timing. In the olfactory bulb and piriform cortex of awake-behaving rodents, odors induce prominent oscillations in the local field potential (LFP) in the beta (15-30 Hz) frequency range. We find that in the temporal domain, while respiration imposes a slow rhythm to olfactory cortical activity, odors evoke fast (15–30 Hz) oscillations in synaptic currents that are coupled to the LFP. Oscillatory excitation precedes inhibition, generating brief time windows for precise and temporally sparse odor-evoked spikes.

Introduction

In sensory cortices receiving balanced excitation and inhibition, excitation precedes inhibition in response to brief impulse-like stimuli. This difference in the relative timing of excitation and inhibition is proposed to shape stimulus selectivity and precisely timed spike output (Priebe and Ferster, 2008; Wehr and Zador, 2003; Wilent and Contreras, 2005). In the mammalian olfactory system, respiratory modulation is a prominent feature governing the time course of odor-evoked activity (Cang and Isaacson, 2003; Litaudon et al., 2003; Margrie and Schaefer, 2003; Rennaker et al., 2007). Here we use *in vivo* cell-attached followed by whole-cell recordings to reveal how the timing of excitatory and inhibitory synaptic input governs odor representations in L2/3 cells of rat primary olfactory cortex. We show that odor-evoked firing activity is coherent with the LFP at the beta band frequency. We also find that odors evoke fast beta frequency oscillations in synaptic activity. Oscillating excitation precedes inhibition, generating a brief (~10 ms) temporal window that restricts spike timing. These results reveal that oscillatory synaptic inputs govern the timing of odor-evoked activity in olfactory cortex.

Results

In whole-cell voltage clamp recordings from L2/3 cells of rat olfactory cortex, we observe phasic recruitment of both excitatory and inhibitory synaptic currents that is coupled to the respiratory rhythm (Fig. 2.3). We wondered a consistent temporal relationship between odor-evoked excitation and inhibition could account for the timing of respiratory-coupled APs (Fig. 3.1A_1). However, aligning odor-evoked synaptic

currents to the respiratory rhythm revealed that inhibition and excitation were temporally overlapping (Fig. 3.1A,B; n=12 cells) and we could not resolve an obvious relationship between synaptic inputs and spikes times.

We found prominent, odor-evoked beta-frequency oscillations (mean=18.0 ± 1.7 Hz, n=10 rats) in the LFP (Fig. 3.2A), consistent with previous studies of behaving and anesthetized rats (Chapman et al., 1998; Lowry and Kay, 2007; Neville and Haberly, 2003). Beta oscillations were qualitatively similar for different odors and coupled to respiration (Fig. 3.2B_1). Simultaneous cell-attached recording of L2/3 cells and the LFP revealed that APs were phase-locked to LFP beta oscillations (Fig. 3.2B). In all cells, odor-evoked APs were coherent with the LFP at beta frequencies (Fig. 3.2C, n=9 cells). Intriguingly, the peaks of peri-oscillation triggered spike histograms (Fig. 3.2D_1) indicated that APs were not coupled to the same phases of the beta oscillation across different cells. Rather, APs in each individual cell were preferentially coupled to specific phases of the LFP oscillation (Fig. 3.2D_2, n=7/9 cells, Rayleigh test, $p < 0.05$). LFP oscillations simultaneously recorded at the most rostral and caudal edges of anterior piriform cortex (~2.5 mm apart) were virtually coincident (lag: 1.2 ms, 0.11 radians), ruling out the possibility that cell specific AP-LFP phase relationships reflected varying distances between the site of LFP and AP recording. Furthermore, in cells that responded with APs to multiple odors (n=3 cells), the AP-LFP phase relationship appeared identical for each odor (data not shown). These results showing precise phase relationships between APs in individual neurons and synchronized network oscillations point to a temporally sparse code for odor representations in olfactory cortex (Laurent, 2002).

Given the tight temporal association between APs and beta oscillations, we examined the relationship between odor-evoked intracellular synaptic responses and the LFP (Fig. 3.3$A_{1,2}$). We found that respiration-coupled barrages of EPSCs and IPSCs were coherent to the LFP at beta frequencies in all cells (Fig. 3.3A_3; n=9, $p<0.05$, coherence confidence limit). LFP-triggered averages of synaptic currents revealed that EPSCs always preceded IPSCs on a brief, millisecond timescale (Fig. 3.3B; average lag=9±0.3 ms). Strikingly, odor-evoked APs were largely confined to the narrow time windows when EPSCs led IPSCs in the same cells (Fig. 3.3C,D; n=3 cells). On average, 67±11% of APs during odor presentation occurred during the LFP period (~ 0.7π, 20 ms) corresponding to the time window between the onset of the EPSC and the 50% rise time of the IPSC. In contrast, only 32±12% of APs occurred during the same length of LFP period (~ 0.7 π) when measured from the onset of IPSC. In addition, only 8±2% of APs occurred during the LFP period (~ 0.4 π, 13 ms) corresponding to the interval from the 50% rise time of the IPSC to the time of its peak. We also found that synaptic excitation and inhibition were always coupled to distinct phases of the LFP beta oscillation in each cell (Fig. 3.3D, n=9 cells), consistent with the cell specific distribution of AP-LFP phases. Thus, while respiration imposes slow epochs of overlapping excitation and inhibition, odors evoke rapidly oscillating synaptic currents. Phase differences in oscillating EPSCs and IPSCs enforce precise spike timing in olfactory cortex.

Discussion

Neuronal oscillations are thought to be an important feature that contributes to the processing of information in cortical networks (Buzsaki and Draguhn, 2004; Salinas and Sejnowski, 2001). Fast rhythmic activity in the LFP is well documented in the olfactory systems of both vertebrates and invertebrates (Adrian, 1942; Chapman et al., 1998; Eeckman and Freeman, 1990; Freeman, 1978; Friedrich et al., 2004; Lowry and Kay, 2007; Neville and Haberly, 2003; Perez-Orive et al., 2002; Wehr and Zador, 2003) and synchronous activity of neural ensembles is proposed to be important for odor coding, discrimination, and learning (Laurent, 2002).

We found that odors evoked respiration-coupled, beta-frequency oscillations in the olfactory cortex LFP. Although the precise mechanisms underlying beta frequency oscillations are unclear, they are thought to involve bidirectional connectivity between olfactory bulb and cortex (Neville and Haberly, 2003) and have been implicated during olfactory behavior (Kay and Stopfer, 2006). We show that while firing activity of individual L2/3 cells is slowly modulated by respiration, spike timing is precisely phase locked to beta frequency oscillations in the LFP. Furthermore, individual cells prefer to spike at difference phases of the LFP beta oscillation. Thus, across the cell population and within each breath, odors evoke spikes that are temporally sparse (Laurent, 2002).

What determines the LFP phase at which individual cells spike? Using whole-cell voltage clamp recordings, we show that cells receive excitatory and inhibitory currents coupled to discrete phases of the beta oscillation cycle. Inhibition always lagged excitation on a millisecond timescale and this temporal offset between oscillating EPSCs and IPSCs generated brief time windows governing spike timing. Thus, despite relatively slow respiratory patterning, rapidly oscillating synaptic activity

enforces precise spike timing in olfactory cortex. Our results suggest that spike timing is important for odor representations in olfactory cortex and raises the intriguing possibility that cell-specific spike timing within active ensembles of L2/3 cells contributes to odor coding in brain regions receiving L2/3 projections.

Intriguingly, many of our findings parallel those obtained in the locust mushroom body (Laurent, 2002), a structure positioned at an equivalent stage of the insect olfactory system, but which shares no obvious homology or evolutionary relationship with the mammalian piriform cortex. The pyramidal cell equivalent in the mushroom body is the Kenyon cell and the similarities include: lifetime and population sparseness of principal cell responses, very low response firing rate deviation from baseline, direct and specific excitatory drive, broadly tuned inhibition, stimulus-triggered bursts of beta-range oscillations, and a phase-delay of inhibition relative to excitation.

Indeed, there are relatively few functional differences across these diverse phyla. In locusts, broadly tuned inhibition of mushroom body Kenyon cells is mediated by feed-forward interneurons located in another region, the lateral horn (Perez-Orive et al., 2002). In the piriform cortex, broadly tuned inhibition is generated locally by feed-forward and perhaps feedback interneurons. While Kenyon cells fire spikes with a similar mean phase relationship to odor-evoked LFPs (Perez-Orive et al., 2002) recorded in the antenna lobe (the equivalent of the mammalian olfactory bulb), we find that the firing phase of individual pyramidal cells relative to the LFP varies across all cells. Overall, the remarkable similarities between the two different systems may reflect

fundamental principles governing the processing of olfactory information in higher brain regions.

Sparse representations of stimuli have been found across a variety of sensory systems (Brecht and Sakmann, 2002; Davison and Katz, 2007; Hahnloser et al., 2002; Hromadka et al., 2008; Margrie et al., 2002; Perez-Orive et al., 2002; Rinberg et al., 2006; Vinje and Gallant, 2000). Sparseness is proposed to promote the efficient coding of sensory information in the brain by having a relatively small fraction of neurons within a large population active at any given time (Hromadka et al., 2008; Laurent, 2002; Olshausen and Field, 2004; Rolls and Tovee, 1995; Willmore and Tolhurst, 2001). Global inhibition and synchronized oscillatory synaptic currents are well suited to generate odor representations in olfactory cortex that are both spatially and temporally sparse.

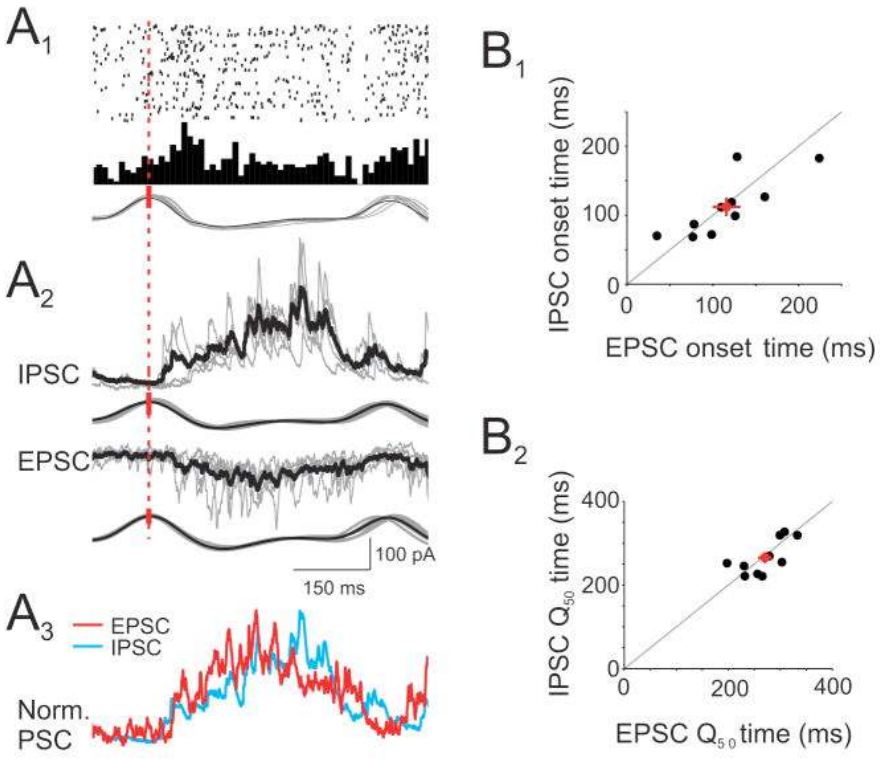

Fig. 3.1 Respiration-coupled synaptic excitation and inhibition. **A_1**, Raster plot (top) and peristimulus time histogram (middle) of odor-evoked APs aligned to respiration (bottom) from one cell. **A_2**, Respiration-triggered average EPSC and IPSC for the cell in A_1. Black trace, average current. Grey traces, single trials. Red dashed line notes the peak of inhalation to which responses were aligned. **A_3**, Normalized respiration-triggered EPSC (red, inverted) and IPSC (blue) have overlapping time courses. **B**, Respiration-triggered EPSCs and IPSCs have similar onset times **B_1**, and time to 50% of charge transfer **B_2**, in individual cells (n=12 cells).

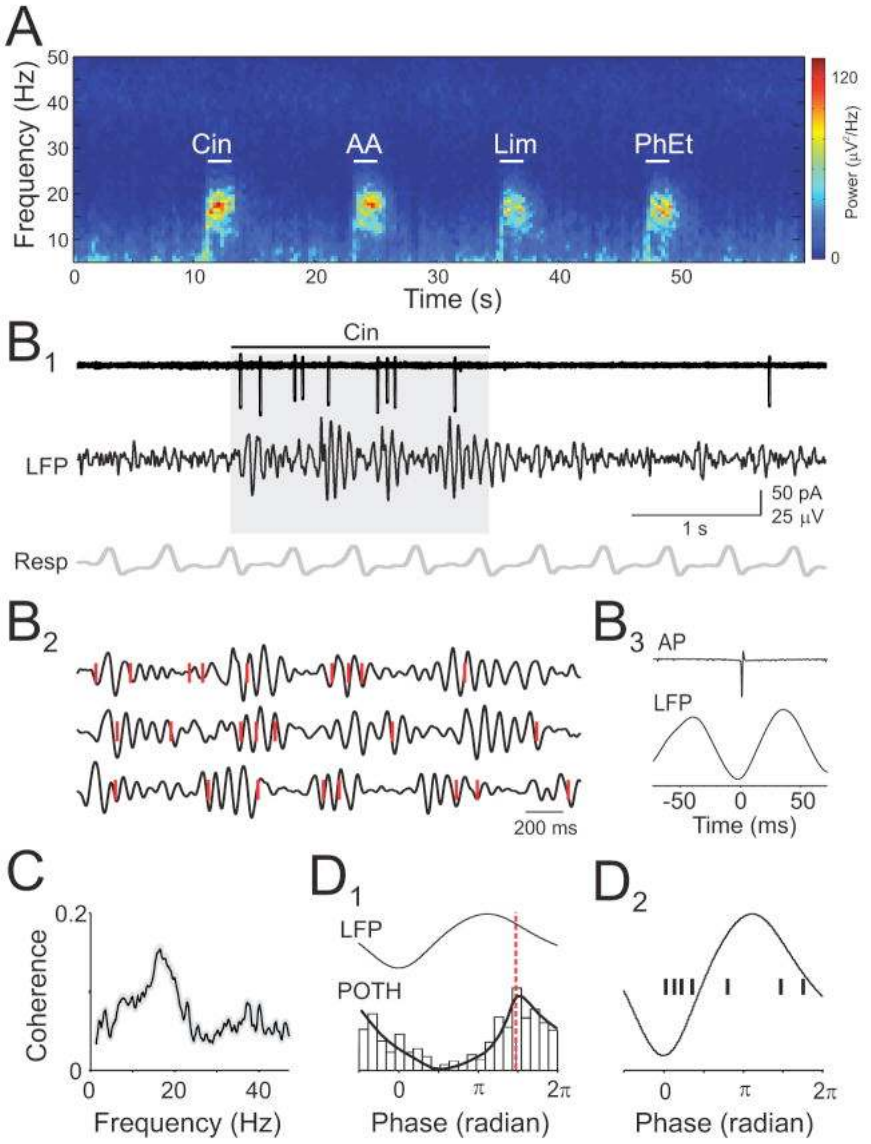

Fig. 3.2 Odor-evoked spikes are phase-locked to beta oscillations. **A**, Spectrogram of an LFP recording showing beta oscillations evoked by four odors. **B_1**, Simultaneously recorded odor-evoked APs (top), LFP (filtered at 5–30 Hz), and respiration. **B_2**, Expansion of grey shaded period in B_1, (top trace) and two other trials. Red ticks indicate APs. **B_3**, Spike-triggered average LFP from the same cell. **C**, Average coherence between odor-evoked APs and LFPs (n=9 cells). **D_1**, Peri-oscillation triggered histogram (POTH) of odor-evoked spikes from cell shown in (B) superimposed with a local linear fit. Red dashed line indicates peak of POTH used to determine AP-LFP phase. **D_2**, AP-LFP phase relationships (black ticks) for 7 cells.

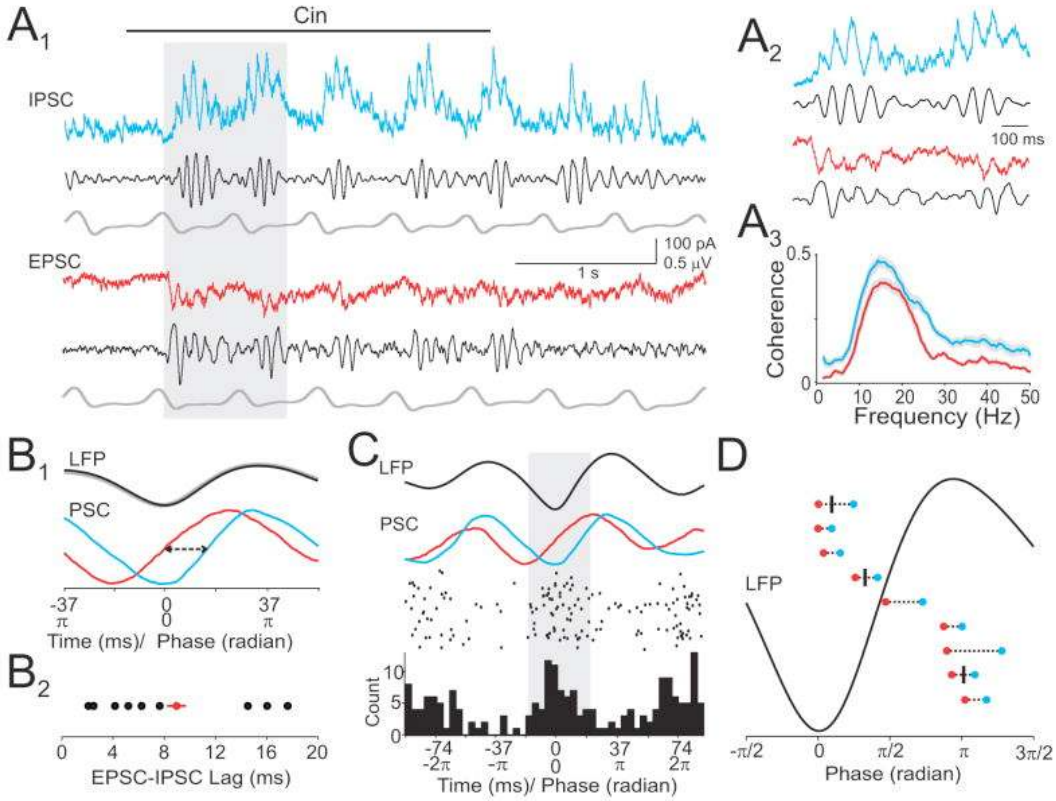

Fig. 3.3 Oscillating EPSCs and IPSCs govern spike timing. **A_1**, Simultaneous recording of synaptic currents and LFP. Grey shaded period is expanded in A_2. **A_3**, Average coherence between odor-evoked synaptic currents and LFPs (n=9 cells). **B_1**, LFP oscillation-triggered average EPSC (red) and IPSC (blue) from cell in A. EPSC is shown inverted. Arrows, lag time measured as interval between EPSC and IPSC 50% rise times (T_{50}). **B_2**, Summary of EPSC-IPSC lag time for 9 cells. **C**, Top traces: LFP and oscillation-triggered EPSC and IPSC. Bottom panels: peri-oscillation triggered raster and spike histogram for the same cell. **D**, Summary of EPSC-IPSC timing relative to LFP phase for 9 cells. Red: EPSC T_{50}, blue: IPSC T_{50}. AP-LFP phase relationships (black ticks) are shown superimposed for the three cells that fired APs in response to odors.

Acknowledgements

This chapter consists of work published in Poo C. and Isaacson, J.S. Odor representations in olfactory cortex: "sparse" coding, global inhibition and oscillations. Neuron. 2009 June 25; 62(6): 850–861. The dissertation author was the primary author of this material.

Chapter 4. Associational input shapes odor-evoked activity in olfactory cortex

Abstract

Stimulus-evoked activity in sensory cortices reflects both excitatory afferent input from the periphery as well as intracortical (lateral excitatory) connections. In primary olfactory (piriform) cortex, layer 2/3 principal cells receive two major sources of excitatory inputs: direct sensory input from mitral cell axons via the lateral olfactory tract (LOT) and associational (ASSN) connections from other cortical pyramidal cells. However, the relative contribution of these two distinct pathways in shaping odor representations in piriform cortex is unclear. Here, we use in vivo whole-cell recordings in anesthetized rats and selective pharmacological manipulation of cortical circuits to examine the contribution of bulbar and ASSN inputs to odor-evoked synaptic excitation. We took advantage of the fact that activation of presynaptic GABAB receptors strongly depresses ASSN transmission with no effect on LOT-evoked responses (Tang and Hasselmo, 1994; Franks and Isaacson, 2006). We show that in piriform pyramidal neurons, ASSN input contributes to a large component of odor-evoked synaptic excitation and broadens the tuning of excitation to a panel of odors. We find that ASSN input in piriform cortex contributes to both the strength and the tuning of odor-evoked excitation.

Introduction

Cortical neurons *in vivo* receive a constant barrage of spontaneous and sensory-driven synaptic inputs from multiple sources. In neocortex, significant effort has been made in differentiating contributions of direct thalamic versus intracortical connections in producing stimulus selectivity. In orientation-selective simple cells in layer 4 of cat primary visual cortex, inactivation of the local cortical circuitry had no effect on the tuning of stimulus-evoked excitation (Ferster et al., 1996; Miller et al., 2001). In addition, in rat primary somatosensory cortex, principal whisker evoked excitation of layer 4 neurons is contributed via direct thalamic input, whereas inhibition and excitation to neighboring whiskers is intracortical (Miller et al., 2001). There are two sources of excitatory synaptic inputs onto neurons in the olfactory cortex: direct sensory inputs from the olfactory bulb via the LOT, and intracortical and recurrent ASSN inputs.

The following experiments are aimed at determining the source of odor-evoked excitatory synaptic transmission in the olfactory cortex. The unique synaptic properties of the olfactory cortex allow us to distinguish between the afferent LOT and recurrent ASSN pathway via activation of $GABA_B$ receptors. Application of the $GABA_B$ agonist baclofen causes a strong presynaptic inhibition of ASSN-mediated excitatory transmission and local inhibitory circuitry with no effect on LOT-mediated EPSCs (Tang and Hasselmo, 1994). Our lab has also verified this finding in brain slice recordings and routinely uses baclofen as a tool to pharmacologically isolate LOT-mediated excitatory transmission (Franks and Isaacson, 2005; Franks and Isaacson, 2006). Here, we take advantage of this approach and use cortical superfusion of

baclofen in vivo to differentiate the contribution of sensory afferent (bulbar) input versus ASSN input to odor-evoked EPSCs. We find that odor-evoked excitation scales with the relative contribution of ASSN input. Neurons with "broadly-tuned" EPSCs receive the most odor-evoked ASSN input, whereas neurons with "narrowly-tuned" EPSCs receive predominantly bulbar input. Thus, we propose that intracortical lateral excitation could serve to powerfully shape odor representations in olfactory cortex.

Results

Associational input contribution scales with odor-evoked EPSC strength

We perform in vivo whole-cell voltage-clamp recordings from layer 2/3 pyramidal neurons in olfactory cortex. We examine odor-evoked synaptic excitation and inhibition by holding the cell at -80mV and +10mV respectively. Next, we superfuse onto the cortex 500μM of the $GABA_B$ receptor agonist baclofen, and monitor the effects of baclofen on both EPSCs and IPSCs. The baclofen-sensitive component of the excitatory response corresponds to the contribution of ASSN inputs, whereas the baclofen-insensitive component corresponds to input directly from bulbar sensory afferents. We alternately monitor odor-evoked IPSCs, to control for the agonist diffusing to the appropriate region of olfactory cortex at a sufficiently high concentration, since IPSCs should be strongly suppressed due to autoreceptors on the local interneurons. Thus, we only categorize EPSC responses after baclofen superfusion onset as "baclofen condition" after we observe strong suppression of IPSCs. In two example cells, we find that baclofen always strongly suppresses synaptic inhibition; while it has differentially affects odor-evoked synaptic excitation (Fig. 4.1). In one

example, washout of baclofen and application of the $GABA_B$ receptor antagonist CGP55845 (5μM) rescued odor-evoked IPSCs (Fig. $4.1B_1$). Thus, we believe the suppression of synaptic transmission in the presence of baclofen is due to its action specifically onto $GABA_B$ receptors.

Across multiple cells that were tested with eight odors, we find that baclofen consistently had a strong suppressive effect on inhibition, while excitatory currents were differentially affected (Fig. 4.2). Thus, we concluded that lateral excitatory connections (ASSNs) contribute to odor-evoked excitation variably for different odor-cell pairs. We wondered what are the factors that shape how much ASSN input contributes to a given odor-evoked response. We find that the strength of total odor-evoked excitatory responses (in control conditions), were correlated with both the amplitude of associational input as well as its fractional contribution to the total response (Fig. $4.3A_1$, A_2). In contrast, we surprisingly do not find a relationship between total odor-evoked synaptic excitation and the contribution of bulbar (baclofen-insensitive; Fig. 4.3B) input. This suggests that the relative strengths of olfactory bulb input for a set of odors onto a cortical neuron do not define the tuning of total odor-evoked excitatory currents.

We also find that there is no correlation between the baclofen-sensitive and baclofen-insensitive excitatory components. These data are particularly interesting, since they imply that for a given odor, there is not a fine scale relationship between the strength of odor-evoked bulbar input and its recruitment of intracortical excitatory connections.

<u>Associational input contribution scales with odor tuning of EPSC</u>

In previous recordings, we found that EPSC odor tuning of L2/3 pyramidal neurons are mostly selective to one or two odors when probed with a panel of eight odors. However, there are a range of EPSC tuning properties across the whole population, and some neurons are broadly tuned to many odors (Fig 2.4A_1). We specifically examined the effects of baclofen on neurons with multiple odor-evoked excitatory responses, since our goal is to determine the effects of baclofen on odor-evoked synaptic excitation.

We find that the effect of baclofen on excitatory synaptic currents seemed to be the strongest on neurons with odor-evoked excitation to many odors. Thus, for a given cell, we examined the relationship between EPSC tuning (the number of odors which produce a significant odor-evoked excitatory synaptic response) and the average strength of ASSN input for the evoked responses (baclofen-sensitive component). We find a strong positive correlation between EPSC tuning and ASSN input strength to evoked responses (Fig. 4.4A_1). This correlation is even more apparent when we examine the relationship between EPSC tuning and fractional contribution of ASSN inputs (Fig. 4.4A_2): ASSN input dominates total evoked responses in broadly-tuned cells, while it contributes to only a small component of total evoked responses in narrowly-tuned cells. In contrast to ASSN input, bulbar afferent input strength does not correlate with EPSC tuning (Fig. 4.4B_1).

These data suggest that the role of ASSN inputs in olfactory cortex is to expand the tuning properties of EPSCs of principal neurons. Indeed, we find that in the presence of baclofen, with only bulbar afferents contributing to EPSC tuning, broadly

tuned cells become more selectively responsive, while cells that were originally narrowly-tuned are not affected (Fig. 4.5).

Discussion

Associational connections in piriform cortex have been postulated to shape odor-evoked activity by anatomical, electrophysiological, and modeling studies (Haberly, 2001; Haberly and Presto, 1986; Hasselmo and Bower, 1990; Johnson et al., 2000; Ketchum and Haberly, 1993a, b; Luskin and Price, 1983a, b). A single electrical shock to the axons of mitral cells in piriform cortex produces a complex series of volleys in the extracellular field potential (Ketchum and Haberly, 1993a). The multiple volleys in the field potential reflect first the activation of mitral cell axons (sensory afferent input) and the resulting synaptic excitation onto cortical neurons, followed by spiking of cortical neurons and the resulting synaptic activity (associational input) from their recruitment (Ketchum and Haberly, 1993a, b). This suggests associational input can be activated by incoming sensory afferents.

Anatomically, each piriform cortical pyramidal neuron sends its axon collaterals to cover a widespread area, making synaptic connections onto a large number of other cells within piriform cortex (>1000; (Johnson et al., 2000). In vivo extracellular recordings also have shown correlated activity between putative principle cell pairs in response to odors in olfactory cortex (Rennaker et al., 2007). These studies all point to an influential role for intracortical connections in odor-evoked activity in piriform cortex. However, the precise contribution of ASSN input has not been examined.

Here, we show that ASSN input in piriform cortex is correlated with the strength

of total odor-evoked excitation, such that large odor-evoke responses are dominated by ASSN input. Intriguingly, the strength of odor-evoked afferent input does not seem to be correlated with the recruitment of ASSN excitation. We believe that this observation points to a lack of fine scale anatomical 'co-tuning' between afferent and intracortical fibers. A 'co-tuning' schema in the narrowest sense would be a senario where cortical neurons only contact each other if they are contacted by the same mitral cell axon. Thus, our results clearly rule out this possibility in the olfactory cortex.

In addition, we find that sensory afferent input provides relatively narrowly tuned EPSCs, whereas ASSN input contributes to broaden odor-evoked excitatory responses to many odors. Thus, in conclusion, we find that intracortical (ASSN) input in piriform cortex contributes to both the strength and the tuning of odor-evoked excitation. These results are significant in providing direct evidence that in addition to bulbar afferent input, associational connectivity significantly shape spike output of cortical neurons, confirming the highly associative anatomy previously observed in pirform cortex (Chen et al., 2003; Haberly, 2001; Haberly and Presto, 1986; Luskin and Price, 1983a, b; ul Quraish et al., 2004; Yang et al., 2004). Our findings imply that modulation and plasticity of ASSN inputs could powerfully influence odor representations in olfactory cortex. This raises the possibility that there are distinct populations of pyramidal cells in olfactory cortex. Narrowly tuned cells could be reliably representing specific odor features from the olfactory bulb, while broadly tuned cells with high convergence of intracortical input could be contributing to odor-detection.

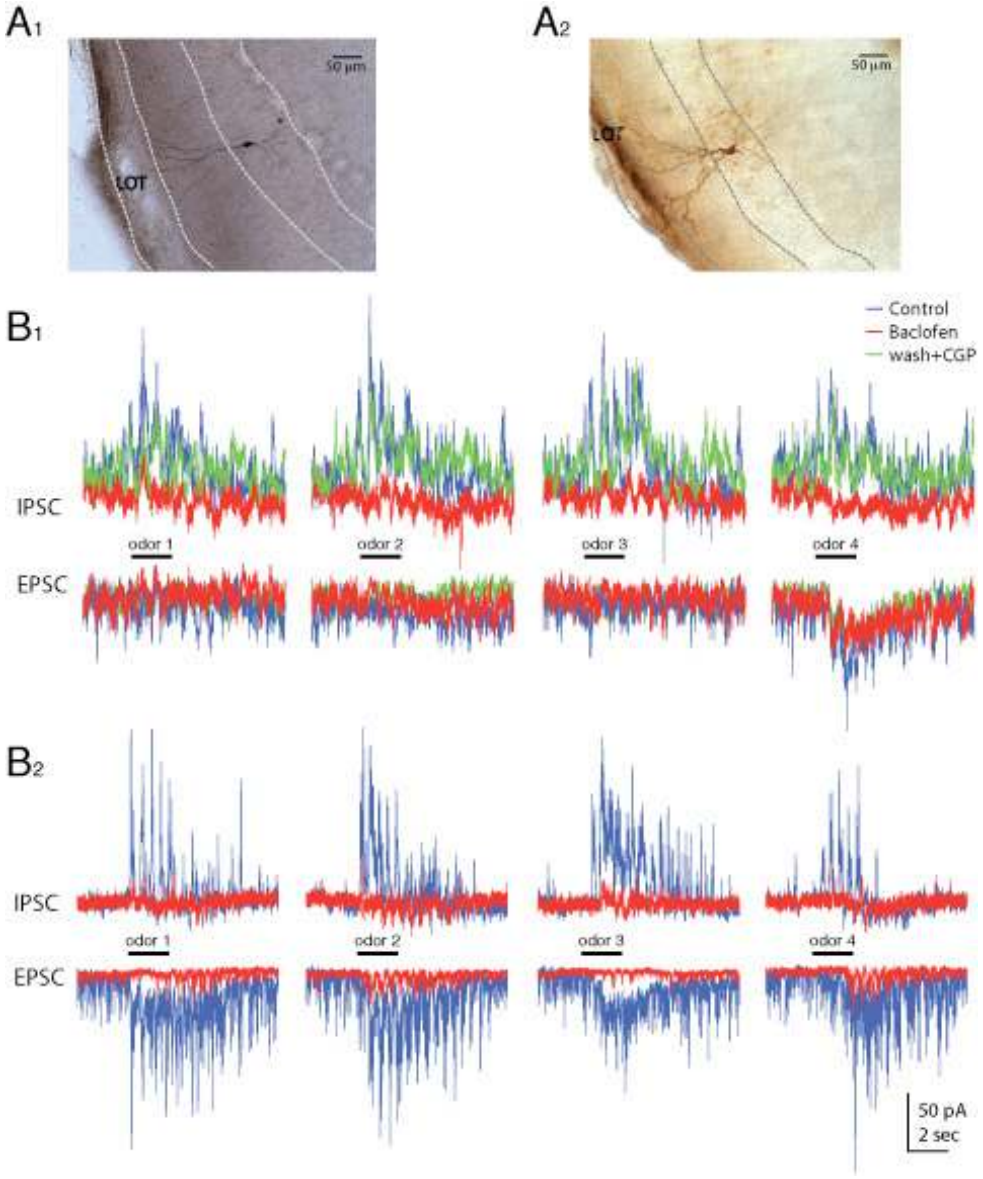

Fig. 4.1 Effects of baclofen on two example L2/3 pyramidal cells. **A_1**, **A_2,** Biocytin filled L2/3 pyramidal neurons in olfactory cortex corresponding to electrophysiological recordings shown in B_1 and B_2, respectively. **B_1**, Recording of a L2/3 pyramidal neuron with odor evoked EPSCs to 1 out of 4 odors (blue traces). Cortical superfusion of 500µM baclofen (red traces) strongly suppressed odor evoked IPSCs, but did not affect odor-evoked EPSC. Recovery of odor-evoked activity was seen with washout of baclofen along with 5µM of CGP55845 (green traces). **B_2**, Recording of a L2/3 pyramidal neuron with odor-evoked activity to all 4 odors. 500µM of baclofen strongly suppressed both odor-evoked IPSCs and EPSCs.

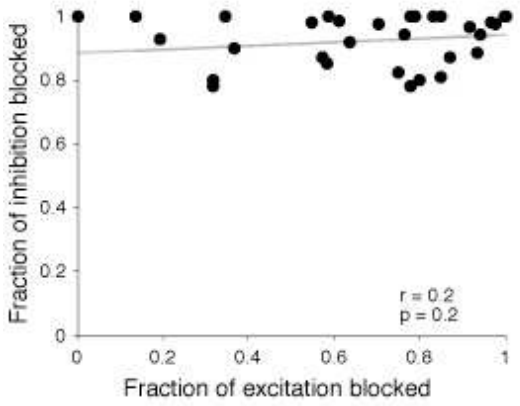

Fig. 4.2 Baclofen differentially affects EPSCs but strongly blocks IPSCs. Each data point is an odor-cell pair in which significant odor-evoked EPSCs were observed in control conditions. Average IPSC charge remaining during the odor presentation in the presence baclofen is 6.09±0.25% of control; average EPSC remaining is 39.96±1.29%. Grey line is fitted linear regression line showing no correlation between fraction of inhibition blocked versus fraction of excitation blocked in baclofen.

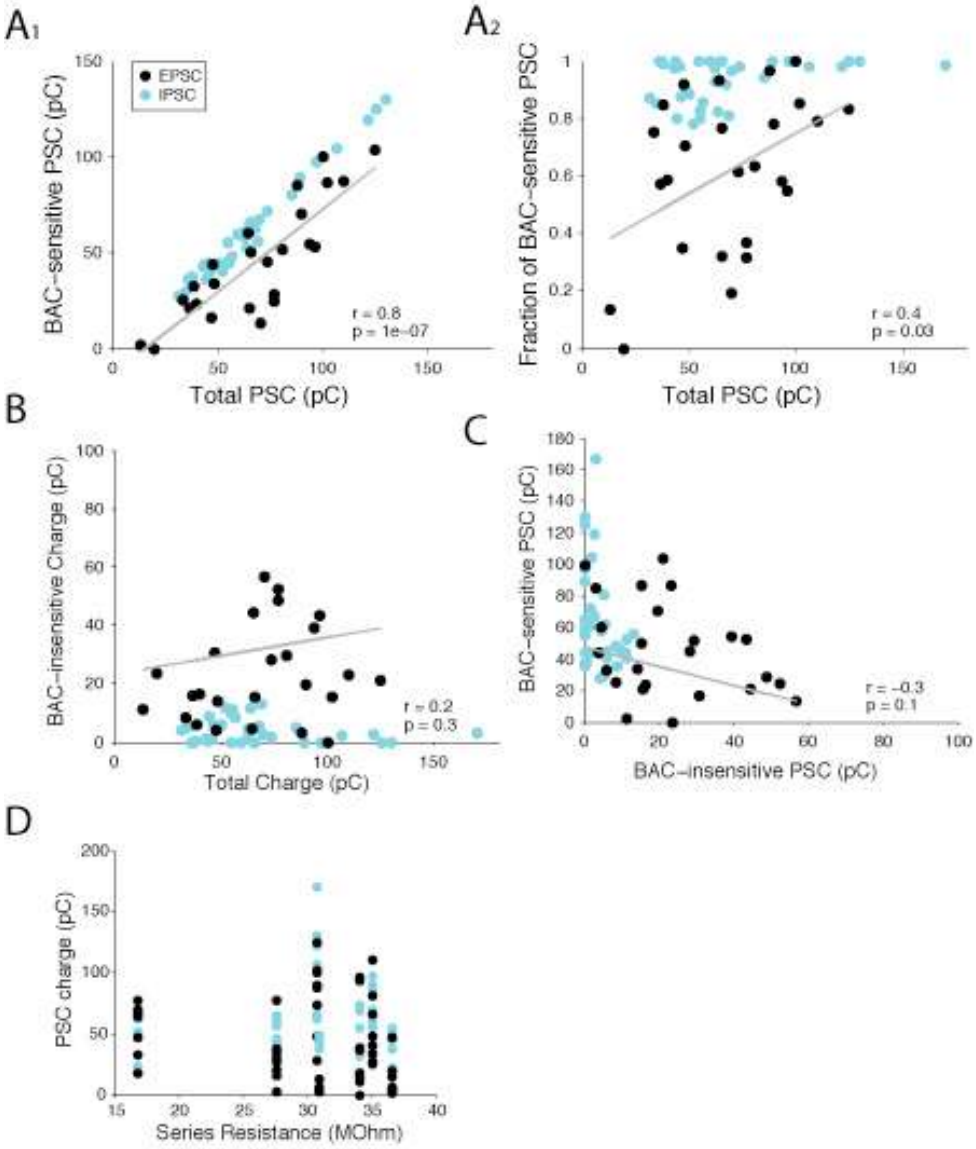

Fig. 4.3 Relative contributions of intracortical and bulbar inputs to total odor-evoked EPSC strength. **A_1,** Baclofen-sensitive (ASSN) EPSCs are correlated to total amount of odor-evoked excitation (black dots). Each data point is an odor-cell pair. **A_2,** The fraction of baclofen-sensitive EPSC (baclofen-sensitive EPSC/ control EPSC) is greater for odor-cell pairs with greater EPSC amplitudes in control conditions. **B,** Baclofen-insensitive (bulbar afferent) input strength is not correlated to total amount of odor-evoked excitation. **C,** there is no correlation between the contributions of intracortical versus sensory afferent input in odor-evoked excitatory responses. **A-C,** Blue dots demonstrate that almost all odor-evoked IPSCs are baclofen-sensitive. **D,** Series resistance does not significantly bias the strength of recorded synaptic currents.

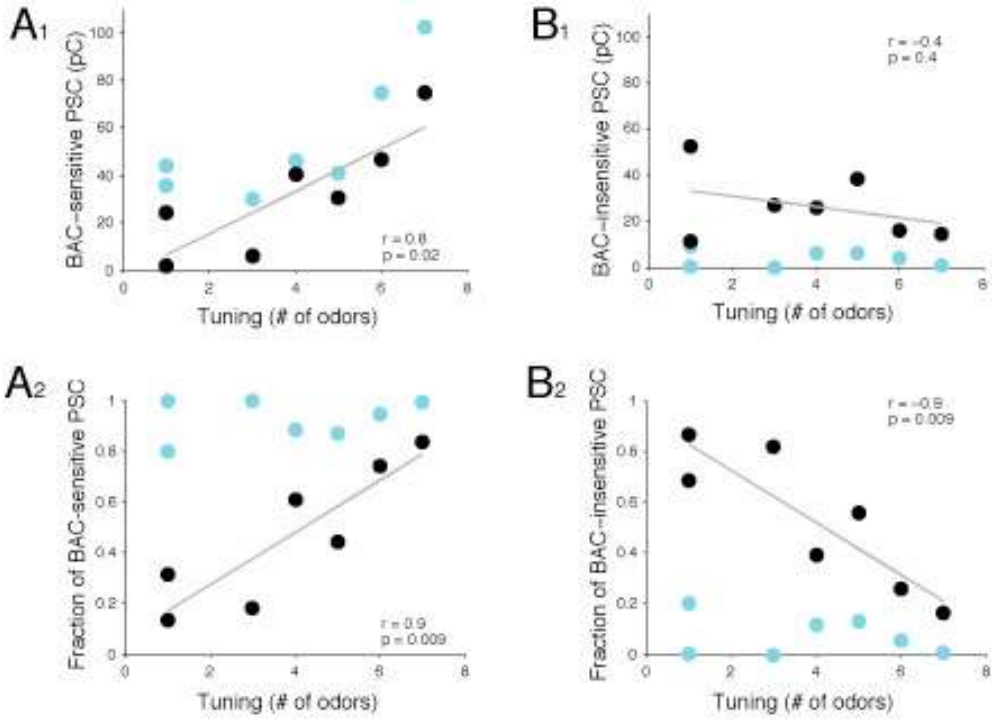

Fig. 4.4 Relative contributions of bulbar and ASSN input to tuning of odor-evoked EPSCs. **A_1,** Each data point is an individual layer 2/3 pyramidal neuron. There is a greater amount of baclofen-sensitive (ASSN) EPSC in neurons that have broadly tuned EPSCs (black). **A_2,** The fraction of baclofen-sensitive EPSC is also greater in broadly tuned cells. **B_1**, There is no correlation between baclofen-insensitive (bulbar afferent) EPSCs strength and tuning of neurons. **B_2,** Mirroring the increase in fractional contribution of ASSN input in neurons with broader EPSC tuning, there is a corresponding decline in the fractional contribution of bulbar afferents. **A, B,** blue dots represent effects of baclofen on IPSCs recorded plotted against EPSC tuning.

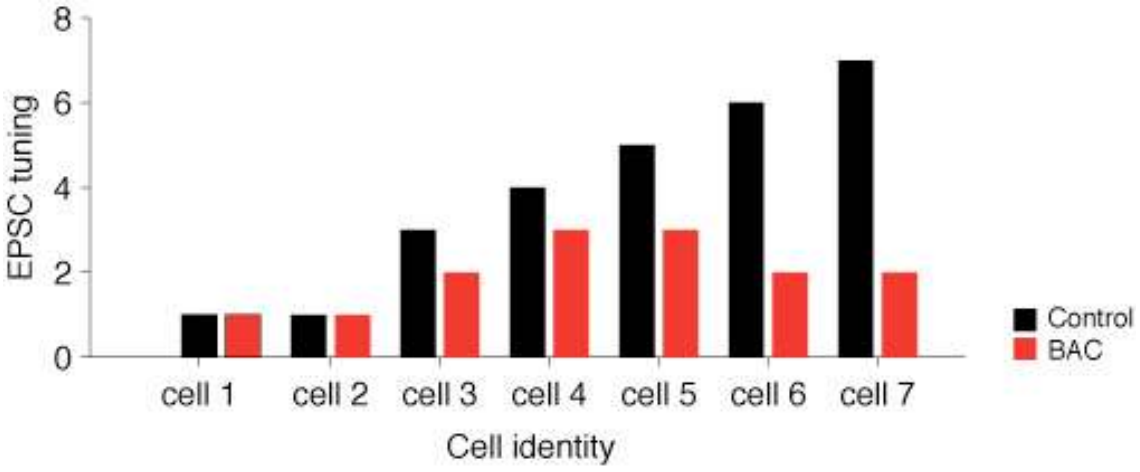

Fig. 4.5 Intracortical input broadens EPSC tuning in pyramidal cells. All 7 cells are histologically identified L2/3 pyramdial cells. Each cell is tested with eight odors. Baclofen (red bars) reduces the number of odors that evokes a significant excitatory response in neurons that are responsive to multiple odors. Odors: cineole, amyl acetate, R-limonene, phenyl ethylalcohol, eugenol, dimethyl pyrzadine, citral, and ethyl butyrate.

Chapter 5. Cortical feedback to olfactory bulb

Abstract

The contribution of cortical feedback to olfactory information processing in the olfactory bulb is unclear. Anatomical studies suggest that these centrifugal fibers densely project to granule cell layer in the olfactory bulb, and could shape activity in the olfactory bulb. Recent advances in optogenetic approaches provide a powerful way to study these fibers, which has been previously impossible. Here, we develop a method to selectively and reversibly silence cortical feedback projections while recording activity in the mouse olfactory bulb. We show that centrifugal input provide excitatory drive onto granule cells, and thus granule cell-mediated inhibition onto mitral/tufted cells.

Introduction

Cortical feedback projects have been the focus of many studies in the past. In particular, the role of V1 projection back to the lateral geniculate nucleau (LGN) of thalamus in shaping receptive fields of LGN cells has been intensely debated (Cudeiro and Sillito, 2006; Sillito and Jones, 2002). The olfactory bulb receives a dense feedback excitatory projection from olfactory cortex pyramidal cells (Haberly and Price, 1978a, b; Luskin and Price, 1983b). These "centrifugal" inputs target the granule cell layer, suggesting that M/T cell inhibition is regulated by a long-range cortical feedback loop (Nakashima et al., 1978). Indeed, in olfactory bulb-cortex slices, stimulation of piriform cortex inputs on the proximal dendrites of granule cells evokes EPSCs and cortical input that drives granule cell action potentials is proposed to gate M/T cell self- and lateral inhibition (Balu et al., 2007; Strowbridge, 2009). This bulbo-cortical loop is also thought to underlie oscillatory dynamics observed in the olfactory bulb and cortex (Gray and Skinner, 1988; Martin et al., 2006; Neville and Haberly, 2003).

Despite the potential importance of centrifugal cortical input in regulating olfactory bulb activity, the role of these projections in olfactory processing is unclear. A barrier to studying cortical inputs (particularly *in vivo*) has been the challenge of selectively and acutely manipulating this pathway. To circumvent this problem, we develop optogenetic approaches to selectively activate and inactivate cortical feedback projections. Specifically, we express halorhoposin (Halo) selectively in L2/3 pyramidal cells in olfactory cortex(Gradinaru et al., 2008). Using activation of Halo, we can record neural activity in the bulb, while reversibly suppressing centrifugal fiber input.

Results

Targeted viral injections in neonatal pups

In order to target viral injections to the olfactory cortex, we first inject the adeno-associated virus (AAV, serotype 2/1) GFP virus into wildtype C57/Bl6 mouse pups. We are able to use landmarks on the lateral surface of the pup's face along with a custom shaped mold to reliably target our injections to olfactory cortex (Fig. 5.1). We allowed the pups to survive for 2 weeks and proceeded to perfuse the brain with fixative. GFP fluorescence was visible in injected hemispheres. The superficial temporal vein and the posterior boarder of the eye were used to triangulate injection sites. We also found that a small volume (~13nl) of injection with multiple injections per site produced the best results. Despite our ability to selectively target our injections sites to the olfactory cortex, we were non-selectively infecting all cells within olfactory cortex. Thus, we chose to take advantage of the cre-dependent vectors to garget halorhodopsin (Halo) to restricted subsets of neurons.

We use Cre-dependent vectors and AAV serotype 2/8 with Halo that is "floxed" by flanking pairs of loxP-type recombination sites. This allowed us to target Halo expression to only neurons expressing Cre recombinase. A high-titer (10^{12}) AAV2/8-Ef1a-DIO-eNpHR 3.0-EYFP (K. Deisseroth) was produced by the U. Penn. Vector Core. We use transgenic mice, Ntsr1-creG209, identified from the GENSAT project that selectively express Cre recombinase in pyramidal cells throughout anterior olfactory cortex, but not other cortical regions (Fig. 5.2B_1). Cre is expressed in pyramidal cells in deep L2 and L3, but not superficial L2 (containing small pyramidal and semilunar cells). Confirming the dense feedback projection of pyramidal cells back

into OB, in a coronal cross section of the OB, cre expression is clearly visible in the granule cell layer (Fig 5.2A_1).

Using this method, we were able to restrict the expression of Halo-YFP to only a subset of pyramidal cells located in L2/3 of the olfactory cortex (Fig. 5.2B, C). More importantly, in the ipsilateral OB of the virally infected olfactory cortex, we observe nicely fluorescent centrifugal fiber terminals in the granule cell layer (Fig.5.2A_2). This suggests that Halo-YFP is successfully transported to the distal axon terminals of pyramidal cells.

Suppression of centrifugal fiber activity by halorhodopsin activation

We next studied the electrophysiological properties of piriform cortex neurons from Ntsr1-cre mice previously injected with AAV-floxed-Halo. We were able to obtain whole-cell recordings from neurons that were virally transfected (YFP-positive; Fig. 5.3A) in slices. Consistent with previous observations (Gradinaru et al., 2008), amber (598 nm) light caused large step-like hyperpolarizations in YFP-positive pyramidal cells (mean 72±7 mV, n=6). In response to current step injection, these neurons exhibited regular spiking patterns (Fig. 5.3B) consistent with L2/3 pyramidal neurons in piriform cortex (Suzuki and Bekkers, 2006). Light-induced hyperpolarizations prevented AP firing in response to current step (Fig. 5.3B). Resting membrane potential and input resistance of

Since we observed prominent YFP positive axon terminals in the granule cell layer, we wondered whether Halo expression in the axon terminals alone could be used to suppress neurotransmitter release from centrifugal fibers within the bulb. To test this

possibility, we made olfactory bulb slices from Ntsr1-cre mice expressing Halo in pyramidal neurons of olfactory cortex (Fig. 5.3C). We recorded centrifugal fiber-evoked EPSCs from granule cells in these slices by placing a stimulating electrode in the granule cell layer. Amber light was interleaved for trials with an EPSC recruited by the stimulating electrode. We find that the amber light pulse was able to strongly suppress the amplitude of nerve-evoked EPSCs under these conditions (Fig. 5.3D). These results indicate that local activation of Halo can suppress excitatory transmission from cortical inputs within the olfactory bulb, presumably by generating sufficient hyperpolarization to block AP invasion of nerve terminals.

To test whether Halo activation in centrifugal terminals can modulate olfactory bulb activity in vivo, we peformed cell-attached recordings from granule and mitral cells from Ntsr1-cre mice expressing Halo in the ipsilateral olfactory cortex. To allow for maximal light activation of centrifugal fibers, we thin the skull over the entire dorsal surface of the bulb. A fiber-coupled LED was positioned <1mm above the craniotomy.

Light caused a rapid reduction in firing rate in a presumptive granule cell (~300 μm from surface) in a Halo-infected mouse (Fig. 5.4A). The light-induced suppression of spontaneous action potentials in this granule cell suggests they were driven by cortical excitatory input. Odor-evoked APs from a presumptive mitral cell (~200 μm from surface) under control conditions and during interleaved trials with light pulses (Fig. 5.4B_1). Consistent with previous reports of M/T cell activity in vivo (Bathellier et al., 2008; Buonviso et al., 2006; Cang and Isaacson, 2003), odor-evoked APs were coupled to the respiration rhythm (Fig. 5.4B2). Intriguingly, amber light increased firing rate of odor-evoked spikes (Fig. 14B). These recordings suggest that inactivation of

cortical projections can reduce granule cell-mediated inhibition and produce an increase in odor-evoked activity of M/T cells.

Discussion

We show that using optogenetic techniques, we can selectively and reversibly silence cortico-bulbar input in mouse olfactory bulb. This is a powerful new method to study the contribution of centrifugal fibers in shaping odor representations in OB. Our recordings from the granule cell layer suggest that centrifugal fibers provide excitatory inputs onto granule cells in the OB. Mitral cells are the main target of granule cell inhibition. Indeed, we find that Halo activation enhances odor-evoked spike output from Mitral cells.

These preliminary results point to a significant role for centrifugal fibers in OB information processing. Granule cell mediated inhibition is a main player governing dendrodendritic self- and lateral inhibition in the olfactory bulb (Balu et al., 2007). This inhibition is thought to be critical for sharpening odor-evoked responses in the olfactory bulb, contributing to odor recognition and discrimination (Abraham et al., 2010). We find that centrifugal fibers appear to be predominately exciting granule cells, suggesting that cortical feedback could enhance odor information processing in the OB. More experiments need to be performed both in slices and in vivo to fully explore the contribution of centrifugal fibers to odor representations in the OB.

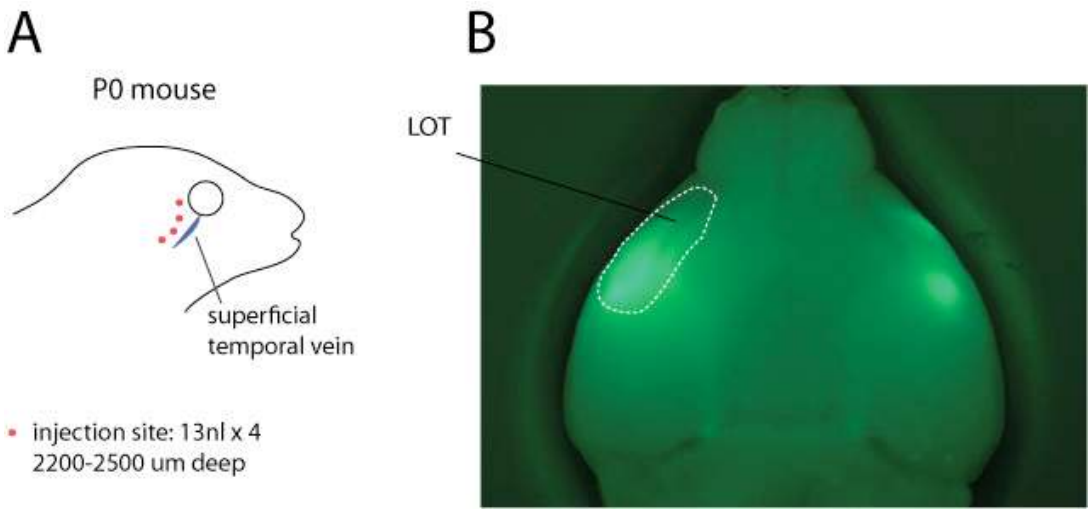

Fig. 5.1 Viral injections in p0 mouse pup successfully infects olfactory cortex. **A,** Schematic of injection sites (red dots) on the lateral surface of a p0 mouse pup skull. The superficial temporal vein and the eye are used as landmarks. **B,** Ventral view of a whole brain. A wildtype mouse was injected at p0 with AAV2/1-GFP. Brain is fixed and visualized 2 weeks after viral injection (p14).

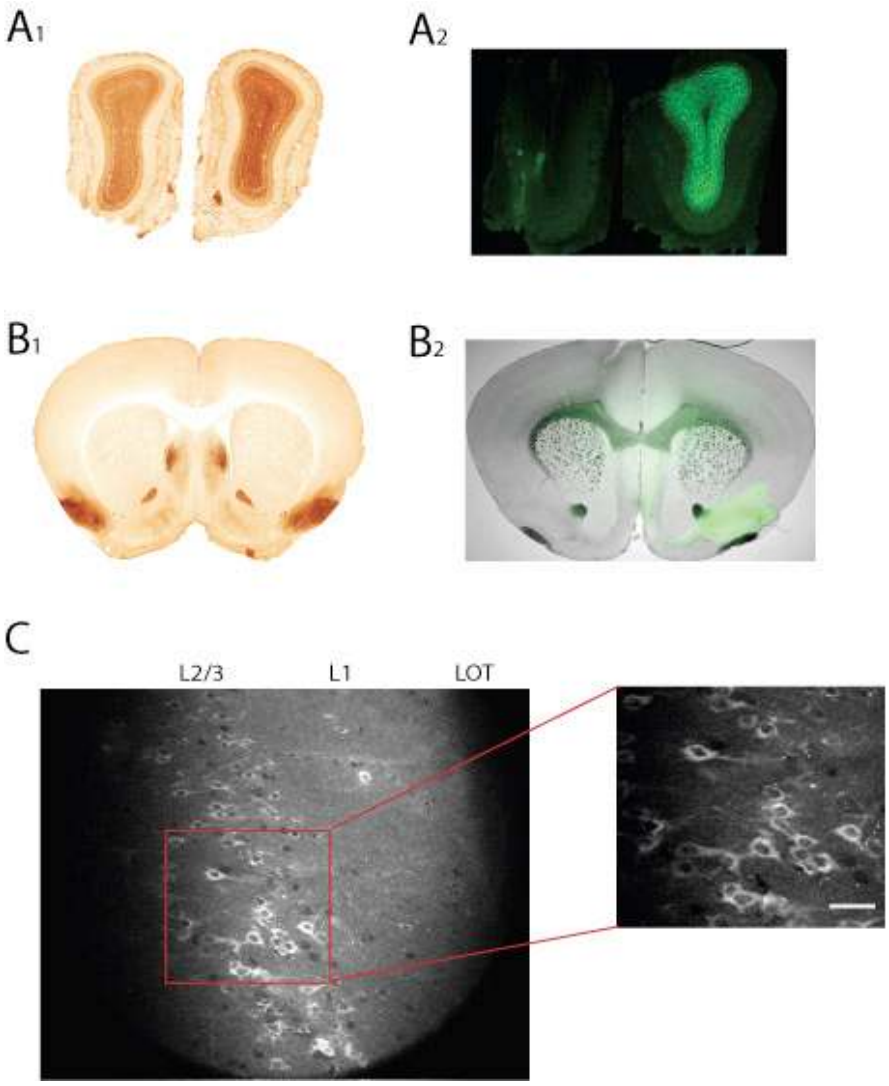

Fig. 5.2 Selective infection of L2/3 pyramidal cells in olfactory cortex. **A_1,** Coronal cross section of an Ntsr1-cre mouse OB, stained for cre expression (http://www.gensat.org). Cre-positive axons of cortical pyramidal neurons (centrifugal fibers) terminate in the granule cell layer. **A_2,** AAV2/8-floxed-eNPHr3.0-EYFP injection in Ntsr1-cre mouse pup infects olfactory cortex L2/3 pyramidal cells. YFP-positive terminals of centrifugal fibers in the ipsilateral OB is visible. **B_1,** Coronal cross section of a Ntsr1-cre mouse, stained for Cre expression (http://www.gensat.org). L2/3 pyramidal cells in olfactory cortex are selectively labeled. **B_2,** AAV2/8-floxed-eNPHr-YFP infection is limited to the right anterior piriform cortex. **C,** A two-photon image of a virally infected olfactory cortical slice. YFP signal can been seen in L2/3 pyramidal neurons. Scale bar is 20μm.

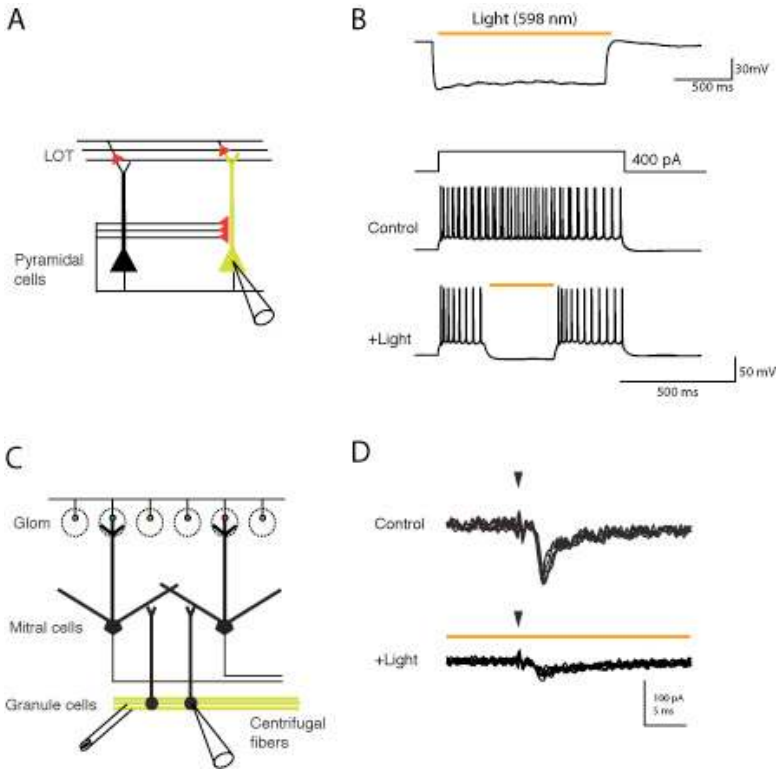

Fig. 5.3 Light activation of halorhodopsin. **A**, Schematic of a recording from a virally infected halo pyramidal cell (yellow) in an olfactory cortical slice. **B**, Activation of halo by amber light (598nm, orange bar) causes hyperpolarization in a YFP-positive pyramidal cell (top trace). Action potentials induced by current injection are blocked by light activation of Halo. **C,** Schematic of a recording from a granule cell in an olfactory bulb slice with viral infection in the ipsilateral olfactory cortex. Stimulating electrode is positioned in granule cell layer to activate cortical input. **D,** Granule cell EPSCs evoked by electrical stimulation (triangles) of cortical inputs are blocked by light. Light onset was 100 ms before stimulation and 200 ms duration. Traces show 5 sweeps overlaid in each condition.

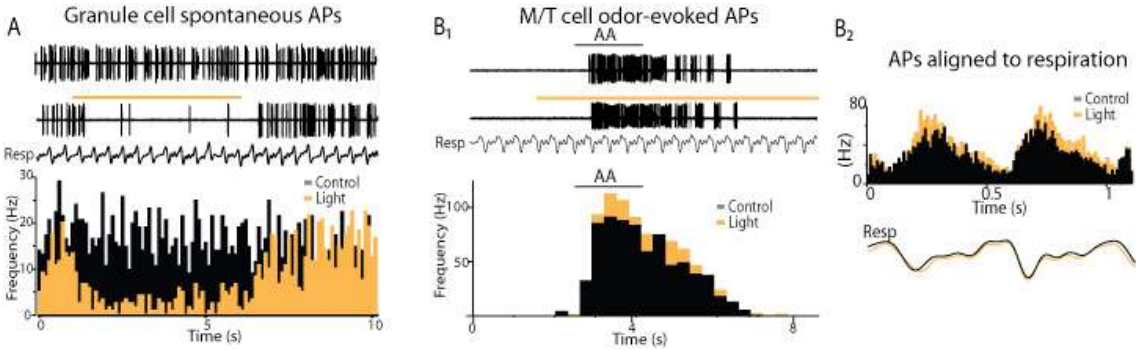

Fig. 5.4 Halorhodopsin-mediated suppression of centrifugal input in vivo. **A,** Cell-attached recording from a granule cell. Spontaneous spiking activity are present in control conditions but are blocked with amber light (592nm, orange bar). Control and light trials are interleaved. Bottom: peristimulus time histogram. **B_1**, Cell-attached recording from a M/T cell. Odor-evoked spiking activity is enhanced by amber light. Control and light trials are interleaved. Bottom: peristimulus time histogram. **B_2**, Action potentials from the same cell aligned to the respiratory rhythm.

Conclusions

Understanding cortical circuits underlying sensory percepts has long been the focus of many studies. Specifically, population activity of neural ensembles, and well as temporal features of the neural responses has been examined in many sensory cortical areas in recent years (Anderson et al., 2000; Brecht and Sakmann, 2002; DeWeese et al., 2003; Hromadka et al., 2008; Murakami et al., 2005; Ohki et al., 2005; Wilent and Contreras, 2005; Zhang et al., 2001). Surprisingly, despite the notable progress made on understanding the peripheral coding of odors (Buck, 1996; Ojima et al., 1984; Rinberg et al., 2006; Rubin and Katz, 1999; Spors and Grinvald, 2002; Uchida et al., 2000; Wachowiak and Cohen, 2001), neural circuits in the olfactory cortex has been largely neglected. It was our goal to begin to address these questions in the olfactory cortex.

Odors activate global inhibition and selective excitation

We first set out to record the population spike output of principle cells in olfactory cortex in response to odor stimuli. We find that odors evoke only a modest increase in spike rate in a small population of neurons. On average approximately 10% of the cortical population is recruited to spike in response to a given odor. Of these neurons, an individual odor evokes on average an increase of only 1.5 spikes per respiratory cycle above baseline activity.

In characterizing the "sparse" population activity of principle neurons, we encountered some central questions: what are the synaptic mechanisms that generate their sparse activity? What features of the cortical circuit shape their spike output? We

chose to address these questions using in vivo cell-attached recordings followed by whole-cell voltage-clamp recordings of the same neurons. This allowed us to compare directly the spike output of an individual neuron with the underlying excitatory and inhibitory synaptic inputs provided by the circuit in which it is embedded.

In response to a panel of odors, we find that inhibitory synaptic input is widely recruited across the cortical population. In addition, in the vast majority of recorded cells, these inhibitory inputs are not selective to odor identity. Thus, we describe the odor-evoked inhibitory response in olfactory cortex as 'global inhibition'. In contrast, we find that excitatory synaptic input is more rarely recruited and is selective to odor identity. Interestingly, we find that across a panel of odors, the odor that evoked the greatest amount of synaptic excitation always corresponded to the odor that evoked spiking activity in the cell-attached recording configuration. Thus, we describe odor-evoked synaptic excitation in olfactory cortex as selective.

When we selectively abolish synaptic inhibition with a low concentration of the $GABA_A$ receptor antagonist gabazine, spiking activity of principle neurons become less selective. We hypothesize that odor-evoked "global" inhibition onto principle cells that we observe in olfactory cortex could be due to a wide recruitment of local inhibitory interneurons by odors. Targeted recordings from layer 1a interneurons supported this hypothesis. We find that these interneurons receive a higher convergence of mitral cell axons, as well as odor-evoke synaptic excitation to a greater number of odors.

These experiments point to a uniquely unbalance recruitment of excitatory and inhibitory circuits in olfactory cortex, such that both selective excitation and global inhibition work together to generate a "sparse" odor code. Indeed further experiments

from our lab demonstrate complimentary sets of inhibitory interneurons in the olfactory cortex that are recruited by afferent input to provide widespread inhibition onto principle cells (Stokes and Isaacson, 2010).

Sparse coding is suggested to be an efficient means for representing sensory stimuli and is advantageous for associative learning (Laurent, 2002; Olshausen and Field, 2004). Thus, this coding scheme is ideal for the olfactory cortex given the immensity of potential odors and its importance for odor learning, recognition, and classification (Wilson et al., 2006). In the insect olfactory system as well as the mammalian olfactory bulb, sparse activity is thought to be critical in the coding of odors (Davison and Katz, 2007; Fantana et al., 2008; Laurent, 2002; Perez-Orive et al., 2002; Rinberg et al., 2006). Our results suggest that sparse coding may be a fundamental strategy of olfactory systems that is highly conserved across diverse species.

Oscillations provide a timing mechanism

Spike timing of neural responses is thought to be important in the coding of sensory stimuli (Borst and Theunissen, 1999; Petersen et al., 2002; Tiesinga et al., 2008). In the olfactory system, odors are known to generate respiratory-coupled neural activity as well as fast oscillatory rhythms as measured by the LFP (Adrian, 1942; Bressler and Freeman, 1980; Buonviso et al., 2006; Chapman et al., 1998; Freeman, 1978). However, little is know about mechanisms that govern these rhythmic temporal features of odor-evoked activity in olfactory cortex.

We find that odors evoke oscillatory activity in the LFP at beta (15-30 Hz) frequency range. In individual neurons, odor-evoked spikes are coherent to the LFP at

the beta frequency. When we obtain whole-cell voltage-clamp recordings from these cells, we find that odor-evoked excitatory and inhibitory synaptic currents are also coherent to the LFP at the beta frequency range. In fact, synaptic excitation leads inhibition on average in each oscillatory cycle, and this time window allows neurons to reach threshold to spike. Thus, a consistent lag in oscillatory synaptic inputs coupled to the LFP allows neurons in olfactory cortex to spike precisely at a particular phase of the LFP oscillation.

It is believed that oscillations play a role in dynamically modulating synchronous activity to facilitate routing of information across cortical areas in a behaviorally relevant manner (Destexhe and Sejnowski, 2001; Engel et al., 2001; Womelsdorf and Fries, 2007). Distinct groups of oscillating neurons can be phase locked at specific times and cooperatively drive postsynaptic targets or be incoherent at other times depending on the nature of sensory stimuli, attentional state, and behavior goals. Beta oscillations in the olfactory bulb and cortex are known to be coherent and can be modulated by behavioral tasks (Freeman, 1978; Lowry and Kay, 2007). Our results demonstrate that excitatory and inhibitory circuits are recruited in a temporally coordinated fashion in olfactory cortex to generate beta oscillation coupled spikes. However, the mechanisms by which these synaptic currents are synchronized both within the olfactory cortex and with the olfactory bulb are unclear require further investigation.

Modulation of cortical odor representations

Olfactory cortex is thought to be the main locus of odor recognition and memory (Haberly, 1998b). Long-term potentiation (LTP) is the most well-established cellular mechanism for learning and memory (Martin et al., 2000). There are two main categories of excitatory glutamatergic contacts onto principle neurons in the olfactory cortex are: bulbar afferents, and intracortical associational fibers. Previous work from our lab established that NMDA receptors are selectively down-regulated at afferent LOT inputs but not ASSN inputs (Franks and Isaacson, 2005), suggesting a potential difference in the ability of these two excitatory pathways to undergo classical NMDA receptor dependent LTP. Indeed, we discover an early critical period for synaptic and structural plasticity of sensory afferent input to the olfactory cortex during the first two postnatal weeks.

In contrast to afferent synapses, we find that ASSN fiber synapses display robust long-term plasticity in mature animals. These inputs may be critical for storing records of previously experienced odors and associating them with past events (De Rosa and Hasselmo, 2000; Haberly, 2001). In computational models of olfactory cortex suggest that associational fibers serve to powerfully influence cortical activity (Haberly, 2001; Hasselmo et al., 1990). Thus, we hypothesized that odor-evoked excitatory input onto principle neurons in olfactory cortex should reflect the recruitment of both bulbar sensory afferents as well as ASSN input.

To our surprise, we find that ASSN input not only contributes to odor-evoked excitation, but it largely determines the EPSC tuning properties of principle neurons. Increased contribution from ASSN input increases the numbers of odors each neuron responds to. In contrast, contribution of bulbar afferent input is similar across all

recorded principle neurons. Our results suggest that while bulbar afferent fibers provide a stable and selective excitatory input to principle neurons in olfactory cortex, plasticity of intracortical ASSN connections could significantly modulate odor response properties of an individual neuron. Together, these findings reveal mechanisms by which the olfactory cortex can both reliably represent odor stimuli and yet be highly capable in forming new odor memories throughout life.

Future explorations in cortical feedback

While we have made progress in understanding the synaptic mechanisms contributing to odor representations in olfactory cortex, there is still considerable work to be done. It has long been known that the olfactory cortex principle neurons provide strong centrifugal feedback projections to the olfactory bulb. How this excitatory loop between the olfactory bulb and cortex contribute to odor coding is unknown and is of great interest to many in the field of cortical circuits and olfaction. This is largely due to the lack of experimental techniques in selectively manipulating this pathway. Using optogenetic methods, we have developed the ability to selectively suppress synaptic transmission from centrifugal fibers. We have only begun preliminary experiments in addressing the role of cortical feedback projections to the OB. Confirming previous anatomical studies (Luskin and Price, 1983b; Nakashima et al., 1978), we find that centrifugal fibers provide excitatory drive onto granule cells. Suppression of these inputs relieved granule-cell mediated inhibition onto mitral cells, resulting in increased odor-evoked spike output.

It would undoubtedly be exciting to continue this line of experiment. Specifically, channelrhodopsin (ChR2) can be expressed in these fibers using similar methods. Activation of ChR2 in OB slices would allow for more careful examination of the postsynaptic targets of centrifugal fibers, as well as its synaptic properties. Complimentary *in vivo* whole-cell voltage clamp experiments would reveal the functional significance of activating or inactivating these inputs in shaping odor-evoked activity onto different cell types.

Furthermore, the cortico-bulbar feedback loop is also thought to be critical in generating and synchronizing odor-evoked beta oscillations in the OB and cortex (Neville and Haberly, 2003). Increased synchronization of oscillatory activity in the OB and olfactory cortex has been demonstrated in animals performing odor discrimination tasks (Chapman et al., 1998; Martin et al., 2004; Ravel et al., 2003). We show previously that oscillatory synaptic activity at beta frequencies is critical in determining spike times of olfactory cortical neurons. Odor-evoked spike times of M/T cells the olfactory bulb have also been shown to be phase-locked to local oscillations (Martin et al., 2004). Thus, we also plan to perform additional experiments to address the functional role of centrifugal fibers in generating and synchronizing odor-evoked beta oscillations in the OB and cortex.

References

Abraham, N.M., Egger, V., Shimshek, D.R., Renden, R., Fukunaga, I., Sprengel, R., Seeburg, P.H., Klugmann, M., Margrie, T.W., Schaefer, A.T., and Kuner, T. (2010). Synaptic inhibition in the olfactory bulb accelerates odor discrimination in mice. Neuron *65*, 399-411.

Adrian, E.D. (1942). Olfactory reactions in the brain of the hedgehog. J Physiol *100*, 459-473.

Andersen, P., Eccles, J., and Voorhoeve, P.E. (1963a). Inhibitory Synapses On Somas Of Purkinje Cells In The Cerebellum. Nature *199*, 655-656.

Andersen, P., Eccles, J.C., and Loyning, Y. (1963b). Recurrent inhibition in the hippocampus with identification of the inhibitory cell and its synapses. Nature *198*, 540-542.

Andersen, P., Eccles, J.C., and Loyning, Y. (1964a). Location Of Postsynaptic Inhibitory Synapses On Hippocampal Pyramids. J Neurophysiol *27*, 592-607.

Andersen, P., Eccles, J.C., and Loyning, Y. (1964b). Pathway Of Postsynaptic Inhibition In The Hippocampus. J Neurophysiol *27*, 608-619.

Anderson, J.S., Carandini, M., and Ferster, D. (2000). Orientation tuning of input conductance, excitation, and inhibition in cat primary visual cortex. J Neurophysiol *84*, 909-926.

Balu, R., Pressler, R.T., and Strowbridge, B.W. (2007). Multiple modes of synaptic excitation of olfactory bulb granule cells. J Neurosci *27*, 5621-5632.

Bathellier, B., Buhl, D.L., Accolla, R., and Carleton, A. (2008). Dynamic ensemble odor coding in the mammalian olfactory bulb: sensory information at different timescales. Neuron *57*, 586-598.

Best, A.R., Thompson, J.V., Fletcher, M.L., and Wilson, D.A. (2005). Cortical metabotropic glutamate receptors contribute to habituation of a simple odor-evoked behavior. J Neurosci *25*, 2513-2517.

Borst, A., and Theunissen, F.E. (1999). Information theory and neural coding. Nat Neurosci *2*, 947-957.

Bower, J.M., and Haberly, L.B. (1986). Facilitating and nonfacilitating synapses on pyramidal cells: a correlation between physiology and morphology. Proc Natl Acad Sci U S A *83*, 1115-1119.

Brecht, M., and Sakmann, B. (2002). Whisker maps of neuronal subclasses of the rat ventral posterior medial thalamus, identified by whole-cell voltage recording and morphological reconstruction. J Physiol *538*, 495-515.

Bressler, S.L., and Freeman, W.J. (1980). Frequency analysis of olfactory system EEG in cat, rabbit, and rat. Electroencephalogr Clin Neurophysiol *50*, 19-24.

Buck, L., and Axel, R. (1991). A novel multigene family may encode odorant receptors: a molecular basis for odor recognition. Cell *65*, 175-187.

Buck, L.B. (1996). Information coding in the vertebrate olfactory system. Annu Rev Neurosci *19*, 517-544.

Buonviso, N., Amat, C., and Litaudon, P. (2006). Respiratory modulation of olfactory neurons in the rodent brain. Chem Senses *31*, 145-154.

Buonviso, N., Revial, M.F., and Jourdan, F. (1991). The Projections of Mitral Cells from Small Local Regions of the Olfactory Bulb: An Anterograde Tracing Study Using PHA-L (Phaseolus vulgaris Leucoagglutinin). Eur J Neurosci *3*, 493-500.

Buzsaki, G., and Draguhn, A. (2004). Neuronal oscillations in cortical networks. Science *304*, 1926-1929.

Cang, J., and Isaacson, J.S. (2003). In vivo whole-cell recording of odor-evoked synaptic transmission in the rat olfactory bulb. J Neurosci *23*, 4108-4116.

Chapman, C.A., Xu, Y., Haykin, S., and Racine, R.J. (1998). Beta-frequency (15-35 Hz) electroencephalogram activities elicited by toluene and electrical stimulation in the behaving rat. Neuroscience *86*, 1307-1319.

Chen, S., Murakami, K., Oda, S., and Kishi, K. (2003). Quantitative analysis of axon collaterals of single cells in layer III of the piriform cortex of the guinea pig. J Comp Neurol *465*, 455-465.

Cudeiro, J., and Sillito, A.M. (2006). Looking back: corticothalamic feedback and early visual processing. Trends Neurosci *29*, 298-306.

Davison, I.G., and Katz, L.C. (2007). Sparse and selective odor coding by mitral/tufted neurons in the main olfactory bulb. J Neurosci *27*, 2091-2101.

de Olmos, J., Hardy, H., and Heimer, L. (1978). The afferent connections of the main and the accessory olfactory bulb formations in the rat: an experimental HRP-study. J Comp Neurol *181*, 213-244.

De Rosa, E., and Hasselmo, M.E. (2000). Muscarinic cholinergic neuromodulation reduces proactive interference between stored odor memories during associative learning in rats. Behav Neurosci *114*, 32-41.

Demir, R., Haberly, L.B., and Jackson, M.B. (1998). Voltage imaging of epileptiform activity in slices from rat piriform cortex: onset and propagation. J Neurophysiol *80*, 2727-2742.

Destexhe, A., and Sejnowski, T.J. (2001). Thalamocortical assemblies : how ion channels, single neurons, and large-scale networks organize sleep oscillations (Oxford ; New York: Oxford University Press).

DeWeese, M.R., Wehr, M., and Zador, A.M. (2003). Binary spiking in auditory cortex. J Neurosci *23*, 7940-7949.

Duchamp-Viret, P., Palouzier-Paulignan, B., and Duchamp, A. (1996). Odor coding properties of frog olfactory cortical neurons. Neuroscience *74*, 885-895.

Eeckman, F.H., and Freeman, W.J. (1990). Correlations between unit firing and EEG in the rat olfactory system. Brain Res *528*, 238-244.

Ekstrand, J.J., Domroese, M.E., Feig, S.L., Illig, K.R., and Haberly, L.B. (2001). Immunocytochemical analysis of basket cells in rat piriform cortex. J Comp Neurol *434*, 308-328.

Engel, A.K., Fries, P., and Singer, W. (2001). Dynamic predictions: oscillations and synchrony in top-down processing. Nat Rev Neurosci *2*, 704-716.

Engert, F., and Bonhoeffer, T. (1999). Dendritic spine changes associated with hippocampal long-term synaptic plasticity. Nature *399*, 66-70.

Fantana, A.L., Soucy, E.R., and Meister, M. (2008). Rat olfactory bulb mitral cells receive sparse glomerular inputs. Neuron *59*, 802-814.

Ferster, D., Chung, S., and Wheat, H. (1996). Orientation selectivity of thalamic input to simple cells of cat visual cortex. Nature *380*, 249-252.

Franks, K.M., and Isaacson, J.S. (2005). Synapse-specific downregulation of NMDA receptors by early experience: a critical period for plasticity of sensory input to olfactory cortex. Neuron *47*, 101-114.

Franks, K.M., and Isaacson, J.S. (2006). Strong single-fiber sensory inputs to olfactory cortex: implications for olfactory coding. Neuron *49*, 357-363.

Freeman, W.J. (1978). Spatial properties of an EEG event in the olfactory bulb and cortex. Electroencephalogr Clin Neurophysiol *44*, 586-605.

Friedrich, R.W., Habermann, C.J., and Laurent, G. (2004). Multiplexing using synchrony in the zebrafish olfactory bulb. Nat Neurosci *7*, 862-871.

Gellman, R.L., and Aghajanian, G.K. (1993). Pyramidal cells in piriform cortex receive a convergence of inputs from monoamine activated GABAergic interneurons. Brain Res *600*, 63-73.

Gradinaru, V., Thompson, K.R., and Deisseroth, K. (2008). eNpHR: a Natronomonas halorhodopsin enhanced for optogenetic applications. Brain Cell Biol *36*, 129-139.

Gray, C.M., and Skinner, J.E. (1988). Centrifugal regulation of neuronal activity in the olfactory bulb of the waking rabbit as revealed by reversible cryogenic blockade. Exp Brain Res *69*, 378-386.

Haberly, L.B. (1969). Single unit responses to odor in the prepyriform cortex of the rat. Brain Res *12*, 481-484.

Haberly, L.B. (1983). Structure of the piriform cortex of the opossum. I. Description of neuron types with Golgi methods. J Comp Neurol *213*, 163-187.

Haberly, L.B. (1998a). Olfactory Cortex. In The Synaptic Organization of the Brain, G.M. Shepherd, ed. (New York: Oxford University Press), pp. 377-416.

Haberly, L.B. (1998b). The synaptic organization of the brain, 4th edn (New York: Oxford University Press).

Haberly, L.B. (2001). Parallel-distributed processing in olfactory cortex: new insights from morphological and physiological analysis of neuronal circuitry. Chem Senses *26*, 551-576.

Haberly, L.B., and Bower, J.M. (1984). Analysis of association fiber system in piriform cortex with intracellular recording and staining techniques. J Neurophysiol *51*, 90-112.

Haberly, L.B., Hansen, D.J., Feig, S.L., and Presto, S. (1987). Distribution and ultrastructure of neurons in opossum piriform cortex displaying immunoreactivity to GABA and GAD and high-affinity tritiated GABA uptake. J Comp Neurol *266*, 269-290.

Haberly, L.B., and Presto, S. (1986). Ultrastructural analysis of synaptic relationships of intracellularly stained pyramidal cell axons in piriform cortex. J. Comp. Neurol. *248*, 464-474.

Haberly, L.B., and Price, J.L. (1978a). Association and commissural fiber systems of the olfactory cortex of the rat. J Comp Neurol *178*, 711-740.

Haberly, L.B., and Price, J.L. (1978b). Association and commissural fiber systems of the olfactory cortex of the rat. II. Systems originating in the olfactory peduncle. J Comp Neurol *181*, 781-807.

Hahnloser, R.H., Kozhevnikov, A.A., and Fee, M.S. (2002). An ultra-sparse code underlies the generation of neural sequences in a songbird. Nature *419*, 65-70.

Hartline, H.K., Wagner, H.G., and Ratliff, F. (1956). Inhibition in the eye of Limulus. J Gen Physiol *39*, 651-673.

Hasselmo, M.E., and Bower, J.M. (1990). Afferent and association fiber differences in short-term potentiation in piriform (olfactory) cortex of the rat. J Neurophysiol *64*, 179-190.

Hasselmo, M.E., Wilson, M.A., Anderson, B.P., and Bower, J.M. (1990). Associative memory function in piriform (olfactory) cortex: computational modeling and neuropharmacology. Cold Spring Harb Symp Quant Biol *55*, 599-610.

Hensch, T.K. (2004). Critical period regulation. Annu Rev Neurosci *27*, 549-579.

Hromadka, T., Deweese, M.R., and Zador, A.M. (2008). Sparse representation of sounds in the unanesthetized auditory cortex. PLoS Biol *6*, e16.

Illig, K.R., and Haberly, L.B. (2003). Odor-evoked activity is spatially distributed in piriform cortex. J Comp Neurol *457*, 361-373.

Jarvis, M.R., and Mitra, P.P. (2001). Sampling properties of the spectrum and coherency of sequences of action potentials. Neural Comput *13*, 717-749.

Johnson, D.M., Illig, K.R., Behan, M., and Haberly, L.B. (2000). New features of connectivity in piriform cortex visualized by intracellular injection of pyramidal cells suggest that "primary" olfactory cortex functions like "association" cortex in other sensory systems. J Neurosci *20*, 6974-6982.

Jung, M.W., Larson, J., and Lynch, G. (1990). Long-term potentiation of monosynaptic EPSPs in rat piriform cortex in vitro. Synapse *6*, 279-283.

Kanter, E.D., and Haberly, L.B. (1990). NMDA-dependent induction of long-term potentiation in afferent and association fiber systems of piriform cortex in vitro. Brain Res *525*, 175-179.

Kanter, E.D., and Haberly, L.B. (1993). Associative long-term potentiation in piriform cortex slices requires GABAA blockade. J Neurosci *13*, 2477-2482.

Kanter, E.D., Kapur, A., and Haberly, L.B. (1996). A dendritic GABAA-mediated IPSP regulates facilitation of NMDA-mediated responses to burst stimulation of afferent fibers in piriform cortex. J Neurosci *16*, 307-312.

Kapur, A., Pearce, R.A., Lytton, W.W., and Haberly, L.B. (1997). GABAA-mediated IPSCs in piriform cortex have fast and slow components with different properties and locations on pyramidal cells. J Neurophysiol *78*, 2531-2545.

Katz, L.C., and Shatz, C.J. (1996). Synaptic activity and the construction of cortical circuits. Science *274*, 1133-1138.

Kay, L.M., and Stopfer, M. (2006). Information processing in the olfactory systems of insects and vertebrates. Semin Cell Dev Biol *17*, 433-442.

Ketchum, K.L., and Haberly, L.B. (1993a). Membrane currents evoked by afferent fiber stimulation in rat piriform cortex. I. Current source-density analysis. J Neurophysiol *69*, 248-260.

Ketchum, K.L., and Haberly, L.B. (1993b). Membrane currents evoked by afferent fiber stimulation in rat piriform cortex. II. Analysis with a system model. J Neurophysiol *69*, 261-281.

Ketchum, K.L., and Haberly, L.B. (1993c). Synaptic events that generate fast oscillations in piriform cortex. J Neurosci *13*, 3980-3985.

Kuan, Y.F., and Scholfield, C.N. (1986). Ca-channel blockers and the electrophysiology of synaptic transmission of the guinea-pig olfactory cortex. Eur J Pharmacol *130*, 273-278.

Kubota, Y., and Jones, E.G. (1993). Co-localization of two calcium binding proteins in GABA cells of rat piriform cortex. Brain Res *600*, 339-344.

Laurent, G. (2002). Olfactory network dynamics and the coding of multidimensional signals. Nat Rev Neurosci *3*, 884-895.

Lebel, D., Sidhu, N., Barkai, E., and Quinlan, E.M. (2006). Learning in the absence of experience-dependent regulation of NMDAR composition. Learn Mem *13*, 566-570.

Leon, M. (1992). Neuroethology of olfactory preference development. J Neurobiol *23*, 1557-1573.

Lin, H., Huganir, R., and Liao, D. (2004). Temporal dynamics of NMDA receptor-induced changes in spine morphology and AMPA receptor recruitment to spines. Biochem Biophys Res Commun *316*, 501-511.

Linster, C., and Hasselmo, M.E. (2001). Neuromodulation and the functional dynamics of piriform cortex. Chem Senses *26*, 585-594.

Litaudon, P., Amat, C., Bertrand, B., Vigouroux, M., and Buonviso, N. (2003). Piriform cortex functional heterogeneity revealed by cellular responses to odours. Eur J Neurosci *17*, 2457-2461.

Lowry, C.A., and Kay, L.M. (2007). Chemical factors determine olfactory system beta oscillations in waking rats. J Neurophysiol *98*, 394-404.

Luna, V.M., and Schoppa, N.E. (2008). GABAergic circuits control input-spike coupling in the piriform cortex. J Neurosci *28*, 8851-8859.

Luskin, M.B., and Price, J.L. (1983a). The laminar distribution of intracortical fibers originating in the olfactory cortex of the rat. J Comp Neurol *216*, 292-302.

Luskin, M.B., and Price, J.L. (1983b). The topographic organization of associational fibers of the olfactory system in the rat, including centrifugal fibers to the olfactory bulb. J Comp Neurol *216*, 264-291.

Maletic-Savatic, M., Malinow, R., and Svoboda, K. (1999). Rapid dendritic morphogenesis in CA1 hippocampal dendrites induced by synaptic activity. Science *283*, 1923-1927.

Marek, G.J., and Aghajanian, G.K. (1996). Alpha 1B-adrenoceptor-mediated excitation of piriform cortical interneurons. Eur J Pharmacol *305*, 95-100.

Margrie, T.W., Brecht, M., and Sakmann, B. (2002). In vivo, low-resistance, whole-cell recordings from neurons in the anaesthetized and awake mammalian brain. Pflugers Arch *444*, 491-498.

Margrie, T.W., and Schaefer, A.T. (2003). Theta oscillation coupled spike latencies yield computational vigour in a mammalian sensory system. J Physiol *546*, 363-374.

Martin, C., Gervais, R., Chabaud, P., Messaoudi, B., and Ravel, N. (2004). Learning-induced modulation of oscillatory activities in the mammalian olfactory system: the role of the centrifugal fibres. J Physiol Paris *98*, 467-478.

Martin, C., Gervais, R., Messaoudi, B., and Ravel, N. (2006). Learning-induced oscillatory activities correlated to odour recognition: a network activity. Eur J Neurosci *23*, 1801-1810.

Martin, S.J., Grimwood, P.D., and Morris, R.G. (2000). Synaptic plasticity and memory: an evaluation of the hypothesis. Annu Rev Neurosci *23*, 649-711.

Mazor, O., and Laurent, G. (2005). Transient dynamics versus fixed points in odor representations by locust antennal lobe projection neurons. Neuron *48*, 661-673.

McCabe, J., and Scholfield, C.N. (1985). Adenosine-induced depression of synaptic transmission in the isolated olfactory cortex: receptor identification. Pflugers Arch *403*, 141-145.

Micheva, K.D., and Beaulieu, C. (1996). Quantitative aspects of synaptogenesis in the rat barrel field cortex with special reference to GABA circuitry. J. Comp. Neurol. *373*, 340-354.

Miller, K.D., Pinto, D.J., and Simons, D.J. (2001). Processing in layer 4 of the neocortical circuit: new insights from visual and somatosensory cortex. Curr Opin Neurobiol *11*, 488-497.

Miller, M., and Peters, A. (1981). Maturation of rat visual cortex. II. A combined Golgi-electron microscope study of pyramidal neurons. J. Comp. Neurol. *203*, 555-573.

Mittmann, W., Chadderton, P., and Hausser, M. (2004). Neuronal microcircuits: frequency-dependent flow of inhibition. Curr Biol *14*, R837-839.

Mittmann, W., Koch, U., and Hausser, M. (2005). Feed-forward inhibition shapes the spike output of cerebellar Purkinje cells. J Physiol *563*, 369-378.

Mombaerts, P. (2001). How smell develops. Nat Neurosci *4 Suppl*, 1192-1198.

Mombaerts, P., Wang, F., Dulac, C., Chao, S.K., Nemes, A., Mendelsohn, M., Edmondson, J., and Axel, R. (1996). Visualizing an olfactory sensory map. Cell *87*, 675-686.

Murakami, M., Kashiwadani, H., Kirino, Y., and Mori, K. (2005). State-dependent sensory gating in olfactory cortex. Neuron *46*, 285-296.

Nakashima, M., Mori, K., and Takagi, S.F. (1978). Centrifugal influence on olfactory bulb activity in the rabbit. Brain Res *154*, 301-306.

Neville, K.R., and Haberly, L.B. (2003). Beta and gamma oscillations in the olfactory system of the urethane-anesthetized rat. J Neurophysiol *90*, 3921-3930.

Neville, K.R., and Haberly, L.B. (2004). The Synaptic Organization of the Brain: Olfactory Cortex, 5 edn (New York: Oxford University Press).

Nicoll, R.A., and Malenka, R.C. (1999). Expression mechanisms underlying NMDA receptor-dependent long-term potentiation. Ann N Y Acad Sci *868*, 515-525.

Ohki, K., Chung, S., Ch'ng, Y.H., Kara, P., and Reid, R.C. (2005). Functional imaging with cellular resolution reveals precise micro-architecture in visual cortex. Nature *433*, 597-603.

Ojima, H., Mori, K., and Kishi, K. (1984). The trajectory of mitral cell axons in the rabbit olfactory cortex revealed by intracellular HRP injection. J Comp Neurol *230*, 77-87.

Olshausen, B.A., and Field, D.J. (2004). Sparse coding of sensory inputs. Curr Opin Neurobiol *14*, 481-487.

Perez-Orive, J., Mazor, O., Turner, G.C., Cassenaer, S., Wilson, R.I., and Laurent, G. (2002). Oscillations and sparsening of odor representations in the mushroom body. Science *297*, 359-365.

Petersen, R.S., Panzeri, S., and Diamond, M.E. (2002). Population coding in somatosensory cortex. Curr Opin Neurobiol *12*, 441-447.

Pouille, F., and Scanziani, M. (2001). Enforcement of temporal fidelity in pyramidal cells by somatic feed-forward inhibition. Science *293*, 1159-1163.

Pouille, F., and Scanziani, M. (2004). Routing of spike series by dynamic circuits in the hippocampus. Nature *429*, 717-723.

Price, J.L. (1973). An autoradiographic study of complementary laminar patterns of termination of afferent fibers to the olfactory cortex. J. Comp. Neurol. *150*, 87-108.

Priebe, N.J., and Ferster, D. (2005). Direction selectivity of excitation and inhibition in simple cells of the cat primary visual cortex. Neuron *45*, 133-145.

Priebe, N.J., and Ferster, D. (2008). Inhibition, spike threshold, and stimulus selectivity in primary visual cortex. Neuron *57*, 482-497.

Quinlan, E.M., Lebel, D., Brosh, I., and Barkai, E. (2004). A molecular mechanism for stabilization of learning-induced synaptic modifications. Neuron *41*, 185-192.

Ravel, N., Chabaud, P., Martin, C., Gaveau, V., Hugues, E., Tallon-Baudry, C., Bertrand, O., and Gervais, R. (2003). Olfactory learning modifies the expression of odour-induced oscillatory responses in the gamma (60-90 Hz) and beta (15-40 Hz) bands in the rat olfactory bulb. Eur J Neurosci *17*, 350-358.

Rennaker, R.L., Chen, C.F., Ruyle, A.M., Sloan, A.M., and Wilson, D.A. (2007). Spatial and temporal distribution of odorant-evoked activity in the piriform cortex. J Neurosci *27*, 1534-1542.

Ressler, K.J., Sullivan, S.L., and Buck, L.B. (1994). A molecular dissection of spatial patterning in the olfactory system. Curr Opin Neurobiol *4*, 588-596.

Rinberg, D., Koulakov, A., and Gelperin, A. (2006). Sparse odor coding in awake behaving mice. J Neurosci *26*, 8857-8865.

Rolls, E.T., and Tovee, M.J. (1995). Sparseness of the neuronal representation of stimuli in the primate temporal visual cortex. J Neurophysiol *73*, 713-726.

Rubin, B.D., and Katz, L.C. (1999). Optical imaging of odorant representations in the mammalian olfactory bulb. Neuron *23*, 499-511.

Salinas, E., and Sejnowski, T.J. (2001). Correlated neuronal activity and the flow of neural information. Nat Rev Neurosci *2*, 539-550.

Satou, M., Mori, K., Tazawa, Y., and Takagi, S.F. (1982). Two types of postsynaptic inhibition in pyriform cortex of the rabbit: fast and slow inhibitory postsynaptic potentials. J Neurophysiol *48*, 1142-1156.

Satou, M., Mori, K., Tazawa, Y., and Takagi, S.F. (1983a). Interneurons mediating fast postsynaptic inhibition in pyriform cortex of the rabbit. J Neurophysiol *50*, 89-101.

Satou, M., Mori, K., Tazawa, Y., and Takagi, S.F. (1983b). Monosynaptic and disynaptic activation of pyriform cortex neurons by synchronous lateral olfactory tract volleys in the rabbit. Exp Neurol *81*, 571-585.

Satou, M., Mori, K., Tazawa, Y., and Takagi, S.F. (1983c). Neuronal pathways for activation of inhibitory interneurons in pyriform cortex of the rabbit. J Neurophysiol *50*, 74-88.

Scholfield, C.N. (1978). Electrical properties of neurones in the olfactory cortex slice in vitro. J Physiol *275*, 535-546.

Scholfield, C.N. (1980). Convulsants antagonise inhibition in the olfactory cortex slice. Naunyn Schmiedebergs Arch Pharmacol *314*, 29-36.

Scholfield, C.N. (1983). Baclofen blocks postsynaptic inhibition but not the effect of muscimol in the olfactory cortex. Br J Pharmacol *78*, 79-84.

Sheldon, P.W., and Aghajanian, G.K. (1990). Serotonin (5-HT) induces IPSPs in pyramidal layer cells of rat piriform cortex: evidence for the involvement of a 5-HT2-activated interneuron. Brain Res *506*, 62-69.

Sheldon, P.W., and Aghajanian, G.K. (1991). Excitatory responses to serotonin (5-HT) in neurons of the rat piriform cortex: evidence for mediation by 5-HT1C receptors in pyramidal cells and 5-HT2 receptors in interneurons. Synapse *9*, 208-218.

Shepherd, G.M.a.G., C.A. (1998). Olfactory Bulb. In The synaptic organization of the brain, G.M. Shepherd, ed. (New York: Oxford University Press), pp. 159-203.

Sillito, A.M., and Jones, H.E. (2002). Corticothalamic interactions in the transfer of visual information. Philos Trans R Soc Lond B Biol Sci *357*, 1739-1752.

Soucy, E.R., Albeanu, D.F., Fantana, A.L., Murthy, V.N., and Meister, M. (2009). Precision and diversity in an odor map on the olfactory bulb. Nat Neurosci *12*, 210-220.

Spors, H., and Grinvald, A. (2002). Spatio-temporal dynamics of odor representations in the mammalian olfactory bulb. Neuron *34*, 301-315.

Staubli, U., Schottler, F., and Nejat-Bina, D. (1987). Role of dorsomedial thalamic nucleus and piriform cortex in processing olfactory information. Behav Brain Res *25*, 117-129.

Stokes, C.C., and Isaacson, J.S. (2010). From dendrite to soma: dynamic routing of inhibition by complementary interneuron microcircuits in olfactory cortex. Neuron *67*, 452-465.

Stripling, J.S., Patneau, D.K., and Gramlich, C.A. (1991). Characterization and anatomical distribution of selective long-term potentiation in the olfactory forebrain. Brain Res *542*, 107-122.

Strowbridge, B.W. (2009). Role of cortical feedback in regulating inhibitory microcircuits. Ann N Y Acad Sci *1170*, 270-274.

Sullivan, R.M. (2003). Developing a sense of safety: the neurobiology of neonatal attachment. Ann N Y Acad Sci *1008*, 122-131.

Suzuki, N., and Bekkers, J.M. (2006). Neural coding by two classes of principal cells in the mouse piriform cortex. J Neurosci *26*, 11938-11947.

Szyszka, P., Ditzen, M., Galkin, A., Galizia, C.G., and Menzel, R. (2005). Sparsening and temporal sharpening of olfactory representations in the honeybee mushroom bodies. J Neurophysiol *94*, 3303-3313.

Tada, T., and Sheng, M. (2006). Molecular mechanisms of dendritic spine morphogenesis. Curr Opin Neurobiol *16*, 95-101.

Tan, A.Y., Zhang, L.I., Merzenich, M.M., and Schreiner, C.E. (2004). Tone-evoked excitatory and inhibitory synaptic conductances of primary auditory cortex neurons. J Neurophysiol *92*, 630-643.

Tang, A.C., and Hasselmo, M.E. (1994). Selective suppression of intrinsic but not afferent fiber synaptic transmission by baclofen in the piriform (olfactory) cortex. Brain Res *659*, 75-81.

Tiesinga, P., Fellous, J.M., and Sejnowski, T.J. (2008). Regulation of spike timing in visual cortical circuits. Nat Rev Neurosci *9*, 97-107.

Tolias, K.F., Bikoff, J.B., Burette, A., Paradis, S., Harrar, D., Tavazoie, S., Weinberg, R.J., and Greenberg, M.E. (2005). The Rac1-GEF Tiam1 couples the NMDA receptor to the activity-dependent development of dendritic arbors and spines. Neuron *45*, 525-538.

Tseng, G.F., and Haberly, L.B. (1988). Characterization of synaptically mediated fast and slow inhibitory processes in piriform cortex in an in vitro slice preparation. J Neurophysiol *59*, 1352-1376.

Turner, G.C., Bazhenov, M., and Laurent, G. (2008). Olfactory representations by Drosophila mushroom body neurons. J Neurophysiol *99*, 734-746.

Uchida, N., Takahashi, Y.K., Tanifuji, M., and Mori, K. (2000). Odor maps in the mammalian olfactory bulb: domain organization and odorant structural features. Nat Neurosci *3*, 1035-1043.

ul Quraish, A., Yang, J., Murakami, K., Oda, S., Takayanagi, M., Kimura, A., Kakuta, S., and Kishi, K. (2004). Quantitative analysis of axon collaterals of single superficial pyramidal cells in layer IIb of the piriform cortex of the guinea pig. Brain Res *1026*, 84-94.

Vassar, R., Chao, S.K., Sitcheran, R., Nunez, J.M., Vosshall, L.B., and Axel, R. (1994). Topographic organization of sensory projections to the olfactory bulb. Cell *79*, 981-991.

Vinje, W.E., and Gallant, J.L. (2000). Sparse coding and decorrelation in primary visual cortex during natural vision. Science *287*, 1273-1276.

Wachowiak, M., and Cohen, L.B. (2001). Representation of odorants by receptor neuron input to the mouse olfactory bulb. Neuron *32*, 723-735.

Wehr, M., and Zador, A.M. (2003). Balanced inhibition underlies tuning and sharpens spike timing in auditory cortex. Nature *426*, 442-446.

Westenbroek, R.E., Westrum, L.E., Hendrickson, A.E., and Wu, J.Y. (1987). Immunocytochemical localization of cholecystokinin and glutamic acid decarboxylase during normal development in the prepyriform cortex of rats. Brain Res *431*, 191-206.

Whitford, K.L., Dijkhuizen, P., Polleux, F., and Ghosh, A. (2002). Molecular control of cortical dendrite development. Annu Rev Neurosci *25*, 127-149.

Wiesel, T.N., and Hubel, D.H. (1963). Effects of visual depreivation on morphology and physiology of cells in the cats lateral geniculate body. Journal of Neurophysiology *26*, 978-993.

Wilent, W.B., and Contreras, D. (2005). Dynamics of excitation and inhibition underlying stimulus selectivity in rat somatosensory cortex. Nat Neurosci *8*, 1364-1370.

Willmore, B., and Tolhurst, D.J. (2001). Characterizing the sparseness of neural codes. Network *12*, 255-270.

Wilson, D.A. (1998a). Habituation of odor responses in the rat anterior piriform cortex. J Neurophysiol *79*, 1425-1440.

Wilson, D.A. (1998b). Synaptic correlates of odor habituation in the rat anterior piriform cortex. J Neurophysiol *80*, 998-1001.

Wilson, D.A. (2000). Odor specificity of habituation in the rat anterior piriform cortex. J Neurophysiol *83*, 139-145.

Wilson, D.A. (2003). Rapid, experience-induced enhancement in odorant discrimination by anterior piriform cortex neurons. J Neurophysiol *90*, 65-72.

Wilson, D.A., Kadohisa, M., and Fletcher, M.L. (2006). Cortical contributions to olfaction: plasticity and perception. Semin Cell Dev Biol *17*, 462-470.

Womelsdorf, T., and Fries, P. (2007). The role of neuronal synchronization in selective attention. Curr Opin Neurobiol *17*, 154-160.

Woolsey, T.A., and Wann, J.R. (1976). Areal changes in mouse cortical barrels following vibrissal damage at different postnatal ages. J. Comp. Neurol. *170*, 53-66.

Yang, J., Ul Quraish, A., Murakami, K., Ishikawa, Y., Takayanagi, M., Kakuta, S., and Kishi, K. (2004). Quantitative analysis of axon collaterals of single neurons in layer IIa of the piriform cortex of the guinea pig. J Comp Neurol *473*, 30-42.

Zhang, L.I., Bao, S., and Merzenich, M.M. (2001). Persistent and specific influences of early acoustic environments on primary auditory cortex. Nat Neurosci *4*, 1123-1130.

Zhang, Y., Burk, J.A., Glode, B.M., and Mair, R.G. (1998). Effects of thalamic and olfactory cortical lesions on continuous olfactory delayed nonmatching-to-sample and olfactory discrimination in rats (Rattus norvegicus). Behav Neurosci *112*, 39-53.

Zou, Z., Horowitz, L.F., Montmayeur, J.P., Snapper, S., and Buck, L.B. (2001). Genetic tracing reveals a stereotyped sensory map in the olfactory cortex. Nature *414*, 173-179.

Zou, Z., Li, F., and Buck, L.B. (2005). Odor maps in the olfactory cortex. Proc Natl Acad Sci U S A *102*, 7724-7729.